
Article:
Udeh, G.T., Michailos, S., Ingham, D. et al. (2020) A techno-enviro-economic assessment of a biomass fuelled micro-CCHP driven by a hybrid Stirling and ORC engine. Energy Conversion and Management, 227. 113601. ISSN: 0196-8904

https://doi.org/10.1016/j.enconman.2020.113601

Conceptual design and dynamic performance evaluation of a biomass fueled micro-CCHP driven by a hybrid Stirling and ORC engine: a techno-enviro-economic assessment.

Godfrey T. Udeh[a,b*], Stavros Michailos[b], Derek Ingham[b], Kevin J. Hughes[b], Lin Ma[b], Mohamed Pourkashanian[b]

a. *Department of Mechanical Engineering, Faculty of Engineering, University of Port Harcourt, Nigeria.*

b. *Energy 2050, Department of Mechanical Engineering, University of Sheffield, Sheffield, S3 7RD, United Kingdom.*

Abstract: Stirling engines (SE) offer good part load performance and high heat sink temperatures which make it a suitable candidate to serve as a prime mover in micro-combined cooling, heating and power (μ-CCHP) applications. In this study, a novel μ-CCHP configuration hybridising a SE prime mover with an ORC to utilise the waste heat from the SE to produce additional power is proposed. Additional waste heat was recovered from the flue gas to dry the biomass feedstock, fire a thermal chiller and produce hot water. Further, a non-ideal thermal model was formulated and implemented in MATLAB to model the SE prime mover while the models of the other subsystems were implemented in Aspen plus®. Also, the control of the subsystems of the μ-CCHP was achieved in MATLAB by establishing a connection between the software and Aspen plus®. A detailed sensitivity analysis was conducted to study the influence of cooling and heating loads, rotational speed of the prime mover and quality of the biomass fuel on the energy utilisation factor, primary energy savings (PES), CO_2 emissions reduction (CO_2ER) and exergy efficiency of the μ-CCHP system. It was found that hybridising SE and ORC increased the power output and thermal efficiency of the standalone SE by 66% and 63.4%, respectively at its operating speed of 2500 rpm, and also improved the performance at high rotational speeds. Further, the deployment of hybrid prime movers in the design of the μ-CCHP yielded high PES and CO_2ER of 55% and 43%, respectively when the system utilised woodchips fuel containing 10% moisture. The proposed energy system performs better than conventional energy systems producing only one energy vector over a wide range of engine frequencies, cooling ratios and woodchips compositions.

Keywords: Poly-generation; Micro-CCHP; Stirling engine; Waste heat recovery; Biomass drying.

1. Introduction

In the face of rapid depletion of energy resources even as the global energy consumption is rising, deliberate efforts are being made to efficiently utilise the available fuel energy. In this regard, contemporary and future energy systems are being configured in the form of a poly-generation energy system to simultaneously generate cooling, heating and electricity, from a single source of fuel energy. These energy systems offer improved performance compared with standalone systems since a single energy source is converted to multiple energy vectors [1]. They could also be installed close to the end-users; thus minimising the losses inherent in transporting useful energy such as electricity or heating, over long distances. For these reasons, poly-generation energy systems are becoming attractive in decentralised energy solutions and are making strong inroads into the European energy mix [2,3]. They are being deployed in the form of a combined heating and power (CHP), cooling and power (CCP) or cooling, heating and power (CCHP) system configurations.

In CHP, CCP and CCHP energy systems, internal and external combustion engines such as Stirling engines, diesel engines, micro-turbines, organic Rankine cycle (ORC) engines and fuel cells [4,5] serve as the prime movers. These prime movers are selected based on the ease of maintenance, cost, electricity, heating and cooling demand, local pollution and electrical efficiency [6]. Among them, the Stirling engine has some fascinating features. Similar to the ORC, it can utilise multiple clean energy sources of low, medium and high grade quality [7]. Stirling engines, however, have good part load performance and high heat sink temperatures [8]. In addition, they produce less noise in operation, low vibration and are easier to maintain [9]. Consequently, Stirling engines have become the subject of intense studies in recent times for deployment in poly-generation. Several recent studies have been undertaken on the modelling and optimisation of decentralised poly-generation energy systems driven by the Stirling engine.

Chahartaghi and Sheykhi [10] compared the energy, exergy, environmental and economic performance of a Stirling engine driven CCHP system working with hydrogen and helium gases. They formulated models to assess the primary energy savings (PES), emissions reduction (ER) and fuel consumption reduction of the system compared with traditional separate cooling, heating and power (SCHP) systems. They found that this system performed better than the conventional SCHP systems especially at low and medium speeds of rotation of the prime mover and for the engine working with hydrogen gas. Similarly, Chahartaghi *et al*. [11] modelled a CCHP energy system comprising two beta-type Stirling engines, a single effect absorption chiller and a domestic water heater. They investigated the tri-generation

primary energy savings (PES) and CO_2 emissions reduction (CO_2ER) of the system as a function of some of the operating and geometrical parameters of the engine and recorded PES and CO_2ER of 29.47% and 36.22%, respectively compared to the conventional SCHP systems. Karami and Sayyaadi [12] evaluated the techno-enviro-economic performance of a Stirling engine driven CCHP system in four different locations with distinct climatic conditions. They reported cost savings in most locations using their proposed system, with the exemption of one location characterised by extremely hot and humid weather.

In principle, the electrical efficiency of a thermal power plant can be enhanced by utilising the onsite available waste heat in another power cycle; this concept is known as topping and bottoming cycle integration. Several ingenious attempts have been made to improve on the performance of the Stirling engine by deploying this approach [13–18].

Balakheli *et al.* [13] evaluated the PES, CO_2ER and fuel cost reduction (FCR) of a CHP system, driven by a hybrid of an IC engine and Stirling engine that utilised the exhaust waste heat from the former. They reported 42% PES, 46.6% reduction in CO_2ER and 79.3% in FCR compared with a CHP system driven by an IC engine only. Bahrami *et al.* [14] reported that combining the Stirling engine with the ORC could yield 4-8% increase in its thermal efficiency. Similarly, Korlu *et al.* [15] deployed a Stirling engine as the bottoming cycle to increase the performance of a gas turbine [15]. They utilised the exhaust of the gas turbine to fire the Stirling engine, which led to improving the efficiency of the gas turbine from 23.6% to 38.85%. Entezari *et al.* [16] conducted energetic, exergetic and economic optimisation of a gas turbine and Stirling engine combined power plant. They found a 16.1% increase in the exergy efficiency, 68.5% increase in the net power output and 10.3% decrease in the levelised cost of energy in the combined power plant compared with the standalone gas turbine plant. The Stirling engine has also been used to improve the electrical efficiency of a solid-oxide fuel cell (SOFC) [17]. Chitsaz *et al*. [17] reported that the energy efficiency of the standalone SOFC system improved by 24.61% by hybridising it with the Stirling engine.

Further, the plant management scheme and the nature of the load a CCHP system is designed to meet have been reported to affect the size and the performance of the system [19–22]. Kaldehi *et al*. [22] modelled an alpha-type Stirling engine driven micro-CCHP system by considering the electrical load following and the thermal load following as the plant management scheme while the overall efficiency was used to determine the capacity of the system. It was found that 40% reduction in CO_2 emissions can be achieved by deploying their energy system, whilst the energy system gave electrical and thermal efficiencies of 34% and 64%, respectively. Maraver *et al*. [20] investigated the impact of cooling ratio, i.e. the ratio of

the cooling load to the sum of the cooling and heating loads on the performance of a CCHP system fired by biomass fuel which will use either the absorption refrigeration system (ABS) or adsorption refrigeration system (ADS) to meet the cooling load demand. The authors reported higher artificial thermal efficiency (ATE) values when the system serviced more of the heating load demand compared with the cooling load.

It is evident that hybridising the Stirling engine with other prime movers such as the ORC could help increase the performance of a standalone Stirling engine and may offer improved performance in a micro-CCHP configuration. However, there are few studies that deployed hybrid Stirling engine and ORC as the prime movers particularly in micro-CCHP systems and examined in details the system's performance at various rotational speeds of the prime mover. In this paper, as our first contribution, we investigate the thermodynamic benefits (power output and efficiency) of deploying hybrid Stirling engine and ORC as the prime movers for a micro-CCHP system at different rotational speeds of the Stirling engine.

Several other research efforts have focused on comparing the performance of micro-CCHP systems when fired by different biomass feed stocks [23–25]. Damirchi*et al.* [23] conducted experiments to investigate the technical viability of using bagasse, pruned wood, poplar, switch grass and saw dust to fire a micro gamma Stirling engine driven CHP plant. They found that saw dust produced the most electrical power when used to fire the engine while pruned wood offered the least power. The authors, however, did not investigate the impact of the quality of the feedstock on the performance of the cogeneration system. Also, Cardozo and Malmquist [24] investigated the impact of fouling of the heaters of the Stirling engine on the performance of a Stirling engine driven micro-CHP plant that is fired by bagasse and woodchips. They found that the plant produced comparable power outputs for both biomass fuels although lower CHP efficiency was achieved when fired with bagasse pellets compared with woodchips because of the higher ash content of the former. Harrod and Mago [25] investigated the performance of a biomass fuel energised CCHP engine driven by a Stirling engine operating at constant efficiency, and meeting constant thermal heat load. They reported cost savings of up to 50% when using woodchips compared with using natural gas.

From the presented literature, woodchips is a promising biomass fuel for firing micro-CCHP systems especially for remote off-grid locations. Unfortunately, in the tropical climates characterised by a fair share of wet and dry seasons, it may be difficult to obtain dry woodchips feedstock all year round. High moisture content is undesirable in woodchips fuel as it could lead to the reduction of the adiabatic combustion temperature of the flue, the

increase in the residence time in the combustion chamber and consequently, a rise in the emissions [26]. To solve this problem, as our second contribution in this paper, we propose in-situ drying of the feedstock with the waste heat from the CCHP. It will be instructive to investigate the impact of achieving different levels of dryness for the woodchips using the exhaust waste heat from the biomass combustor on the performance of a micro-CCHP plant driven by a hybrid Stirling engine and ORC prime mover. To the best of our knowledge, there are no available records of studies in the literature, commissioned to fill this vital research gap.

Therefore, for the first time we investigate the detailed dynamic performance of a beta Stirling engine driven CCHP system with an ORC as the bottoming cycle, and utilising the exhaust waste heat to dry the biomass feedstock, produce cooling in an ARS and hot water in a domestic boiler. This study has four main pillars: concept development, modelling, assessment and interpreting of results through a sensitivity analysis.

The new innovative contributions of this study relative to previous studies are summarised in the following points:

- Proposing a novel CCHP configuration with a hybrid prime mover: Stirling engine and ORC; for combined power generation.
- Recovering exhaust waste heat from the Stirling engine cooler; to produce additional power from the ORC bottoming cycle and from the absorber and condenser of the thermal cooler, and the degraded waste flue; to simultaneously produce cooling and heating.
- Investigating the impact of the cooling ratio on the primary energy savings, exergy efficiency, energy utilisation factor, artificial thermal efficiency, and CO_2 emissions reduction of the novel CCHP system at different rotational speeds of the Stirling engine prime mover.
- Studying the impact of the quality of the biomass fuel on the system's key performance indicators at different cooling ratios and rotational speeds of the prime mover.

This paper has been structured as follows: In Section 2, we present the schematic of the proposed micro-CCHP and describe the modes of operation of the system. In section 3, the mathematical models of the subsystems of the proposed system are formulated and the algorithm for their integration is presented. Section 4 presents the validation of the subsystems of the proposed micro-CCHP. While in Section 5, we present the main results of this study for the thermodynamic benefits of hybridising Stirling engine and ORC and the sensitivity analysis that examines the impact of the cooling ratio and quality of the biomass

169 on the system's key performance indicators. Finally, in Section 6, we present the concluding
170 paragraphs of this paper stating the key findings and its application.

171 2. Description of Hybrid Stirling and ORC micro-CCHP

172 In this section, we present the detailed description of the micro-CCHP (μ-CCHP) system,
173 showing how the subsystems are connected in a process diagram. The decentralised μ-CCHP
174 system comprises six main subsystems which are: biomass dryer (BMD), biomass combustor
175 (BMC), Stirling engine (SE), organic Rankine cycle (ORC), single effect vapour absorption
176 refrigerator (VAR) and domestic water heater (DWH). The system components are
177 represented in the process diagram shown in Fig. 1 and Fig. 2, while Fig. 3 is the
178 thermodynamic process diagram of the hybrid SE and ORC engine. The SE prime mover is a
179 beta-type engine with a rated power of 3 kW while the ORC engine has a rated power of 2.2
180 kW.

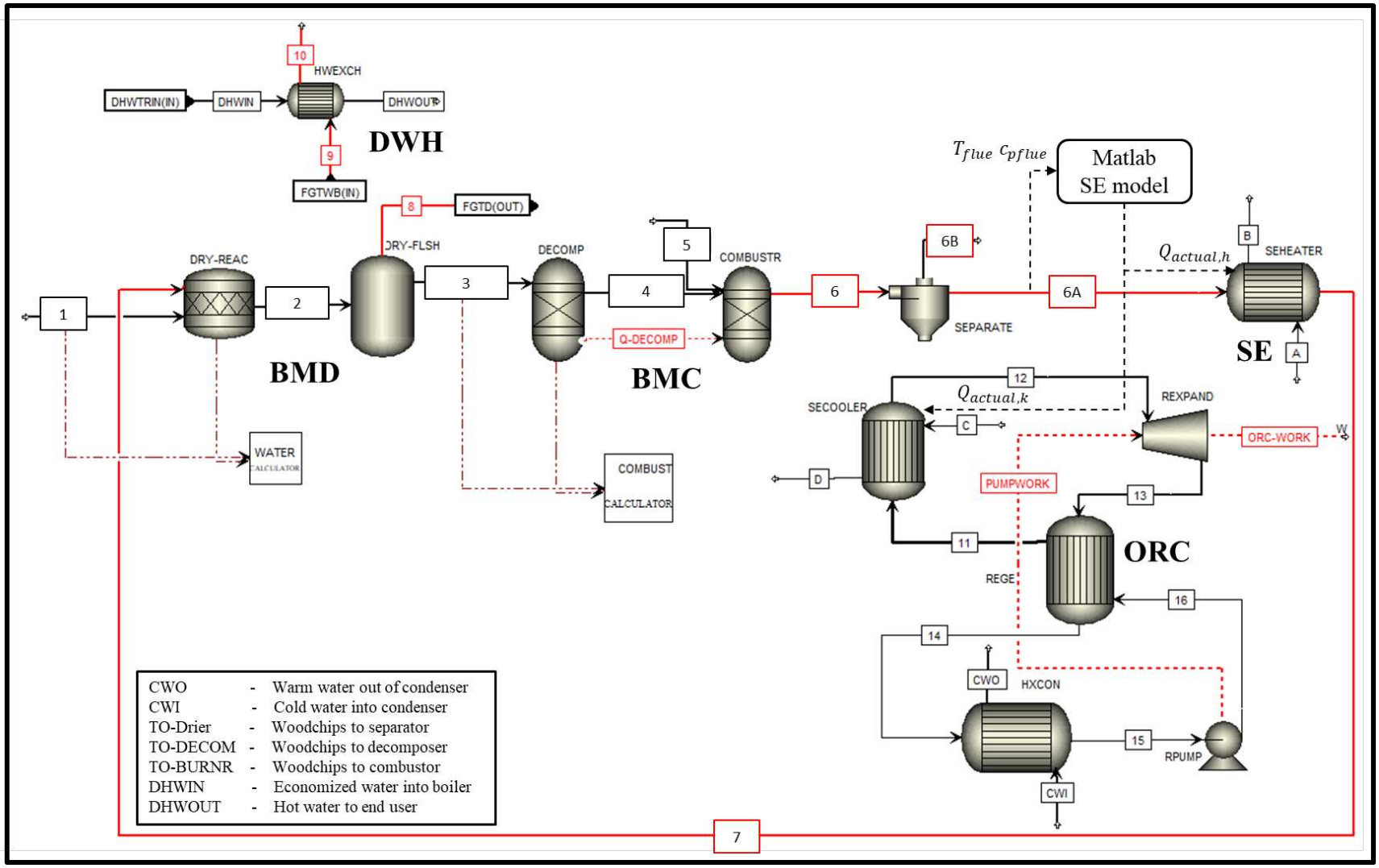

Fig. 1. Schematic of the proposed hybrid Stirling engine and ORC bottoming cycle driven μ-CCHP system.

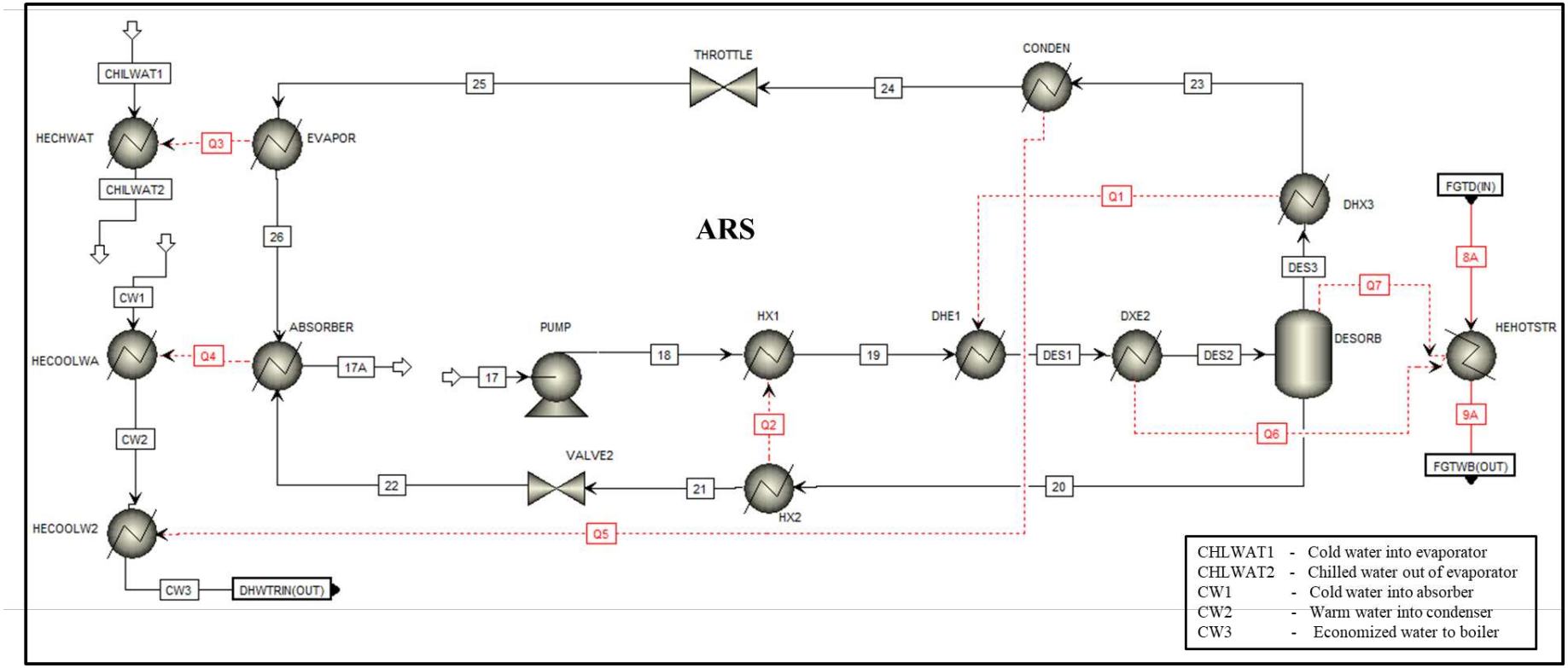

Fig. 2. Process diagram of the single effect vapour absorption system.

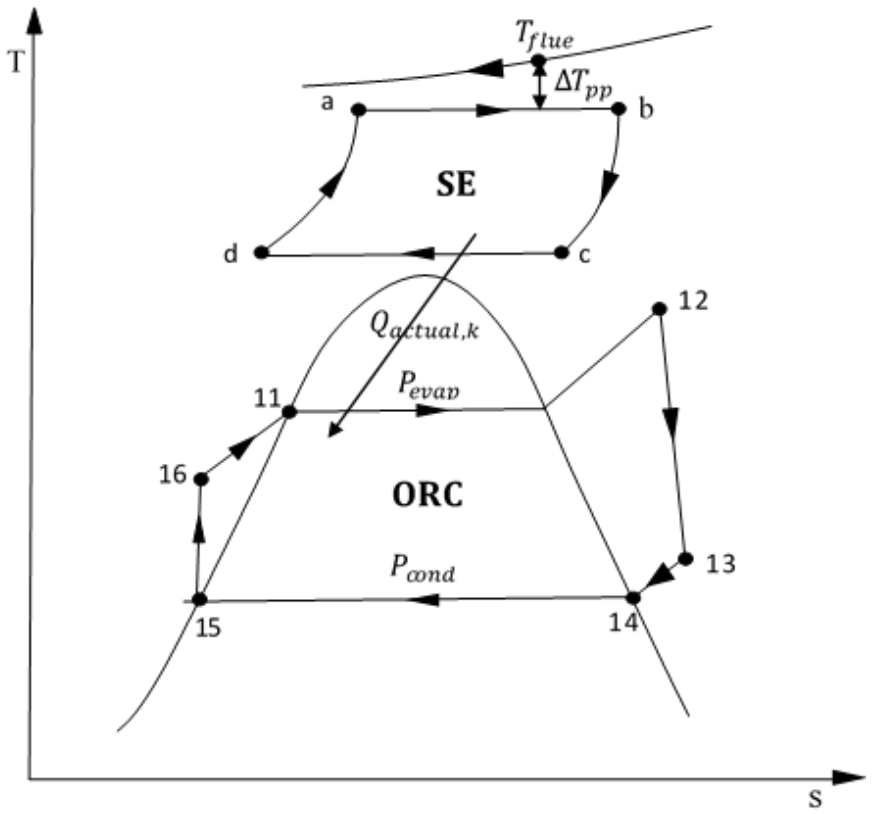

Fig. 3. TS diagram of the theoretical hybrid Stirling and ORC engine cycle.

Woodchips is admitted into the BMD at state 1 and dried using degraded waste flue exiting the SE heater (state 7). At the end of the drying process, the resulting dry woodchips now at state 3 is fed into the BMC, where it mixes with inducted air, at state 5 and is combusted. The flue produced after combustion at state 6B is piped in counter flow to the SE heater. It heats up the working fluid in the tubes of the SE heater and exits the heater at state 7. Meanwhile, the waste heat rejected by the SE cooler during the engine's isothermal process is readily absorbed by the organic working fluid of the ORC, in a cooler/evaporator configuration. This waste heat is used to vaporise the working fluid of the ORC which then drives the blades of the turbine to produce additional electric power. The hybridisation of the SE and ORC yields a combined power configuration that is intended to improve and stabilise the electrical power and efficiency of the prime mover over its operating speeds. The low quality waste heat after the drying process at state 8 is piped to the desorber of the ARS to heat up the lithium bromide-water solution and produce some cooling in the evaporator of the thermal chiller. It is then sent to heat water in the DWH at state 9 before going to stack at state 10. In this design, the water sent to the DWH is pre-heated by picking-up the waste heat from the absorber and condenser of the ARS, which serves as an economizer.

The system described so far has been designed to minimise the loss of useful exergy in the system. Hence, it is expected to yield improved thermodynamic, economic and environmental benefits.

3. Formulating the mathematical models

Here, the mathematical models required to predict the performance of the subsystems of the μ-CCHP will be developed stating the assumptions made. Only the mathematical models for the SE are presented in this section. The models and solution approach implemented for the ORC, ARS, woodchips drying, combustion and domestic hot water production will be presented in a later section.

3.1. Stirling engine model

In a previous study, Udeh *et al*. [27] developed a non-ideal thermal model of the Stirling engine to predict the performance of the experimental engine. This model is obtained by coupling the losses in the engine to the ideal adiabatic model. In this study, the following assumptions were made to develop the model:

- The thermodynamic processes in the engine attained steady state at the end of a cycle of its operation.
- The engine is operating at a fixed speed.
- The working fluid is treated as a perfect gas and obeys the ideal gas law.
- The potential and kinetic energy of the working fluid exerts the same influence at the inlet and outlet of a control volume.
- The heater and cooler are maintained at a constant temperature as it exchanges heat with the working fluid.

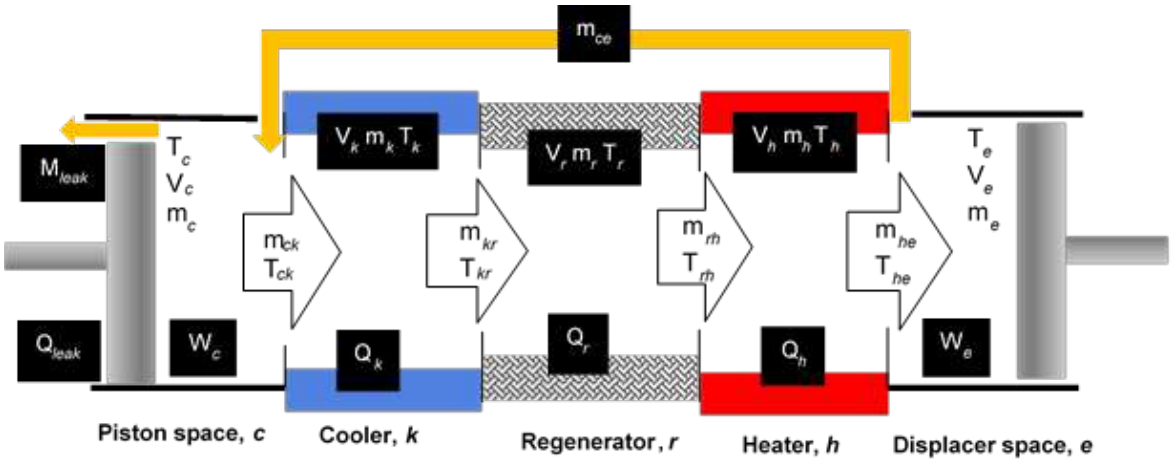

Fig. 4. Schematic diagram of the control volumes of a typical Stirling engine [28].

The SE has been divided into five control volumes (CV) which includes the piston (cold) space, cooler, regenerator, heater and displacer (hot) space, represented in the schematic (Fig. 4) by single suffixes, *c, k, r, h and e,* respectively. In addition, double suffices, *ck, kr, rh, he, ce, and leak* represent the interfaces between the cold space – cooler, cooler – regenerator, regenerator – heater, heater – hot space, hot space – cold space and leakage into the crankcase, respectively. The equation of state, mass and energy conservation principles have been applied to each of the CVs to obtain the instantaneous flow of internal energy in the engine components.

The flow energy equation applied to any CV if we account for the losses in energy due to the pressure drop in the heat exchangers, leakage of energy into the crankcase, shuttle heat loss, leakage of energy via the displacer clearance, and several other work losses is given as [27]:

$$\begin{aligned}\left\{\frac{\delta}{\delta t}\left(Q_{\text{ideal,j}} - Q_{\text{sh}} - Q_{\text{disp}} - Q_{\text{cond}} - Q_{\text{r,non-ideal}} - Q_{\text{leak}}\right)\right\} \\ = \Big\{\left(\dot{m}_{\text{i}} c_{p,\text{i}} T_{\text{i}} - \dot{m}_{\text{o}} c_{p,\text{o}} T_{\text{o}}\right) \\ + \frac{\delta}{\delta t}\left(W_{\text{ideal,j}} - W_{\text{mech.fric.}} - W_{\text{FST}} - W_{\text{hyst.}} - W_{\text{pdrop}}\right) \\ + c_v \frac{d}{dt}(mT)\Big\}\end{aligned} \tag{1}$$

Based on Eq. (1) and other constitutive equations, the set of governing differential equations of the SE have been developed and summarised in Table 1.

The term, $\frac{\delta Q_{\text{sh}}}{\delta t}$ which is the instantaneous rate of heat loss by conduction as a result of the shuttle of the displacer from the hot space to the cold space is given as [29,30]:

$$\frac{\delta Q_{\text{sh}}}{\delta t} = \frac{0.4 {Z_{\text{d}}}^2 k_{\text{d}} D_{\text{d}}}{J_{\text{d}} L_{\text{d}}} (T_{\text{e}} - T_{\text{c}}) \tag{2}$$

On the other hand, the mass loss through the displacer gap into the cold space, $\dot{m}_{\text{ce}}$ and that lost to the crankcase of the engine, $\dot{m}_{\text{leak}}$ have been expressed respectively as [31,32]:

$$\dot{m}_{\text{ce}} = \pi D_{\text{d}} \frac{p}{4 R_{\text{g}} T_{\text{ce}}} \left(U_{\text{d}} J_{\text{d}} - \frac{J_{\text{d}}^3}{6\mu_{\text{g}}} \frac{\Delta p_{\text{ce}}}{L_{\text{d}}}\right) \tag{3}$$

$$\dot{m}_{\text{leak}} = \pi D_{\text{p}} \frac{p + p_{\text{buffer}}}{4 R_{\text{g}} T_{\text{g}}} \left(U_{\text{p}} J_{\text{p}} - \frac{J_{\text{p}}^3}{6\mu_{\text{g}}} \frac{p - p_{\text{buffer}}}{L_{\text{p}}}\right) \tag{4}$$

Eqs. (2) - (4) which model the first category losses in the engine were coupled to the traditional adiabatic equation, resulting in the set of equations presented in Table 1.

Table 1. Governing equations of the non-ideal thermal model of the Stirling engine [27].

$P = \frac{m_t R_g}{\left[\frac{V_c}{T_c} + \left(\frac{V_k}{T_k} + \frac{V_r}{T_r} + \frac{V_h}{T_h}\right) + \frac{V_e}{T_e}\right]}$	Total pressure of the working fluid
$dp = \frac{\frac{\delta Q_{\mathrm{sh}} - \frac{c_p}{R_g} p dV_{\mathrm{c}} - c_p T_{\mathrm{ce}} dm_{\mathrm{ce}}}{c_p T_{\mathrm{ck}}} - \frac{\delta Q_{\mathrm{sh}} + \frac{c_p}{R_g} p dV_{\mathrm{e}} - c_p T_{\mathrm{ce}} dm_{\mathrm{ce}}}{c_p T_{\mathrm{he}}} + dm_{\mathrm{leak}}}{\frac{V_{\mathrm{c}}}{\gamma T_{\mathrm{ck}}} + \frac{V_{\mathrm{k}}}{T_{\mathrm{k}}} + \frac{V_{\mathrm{r}}}{T_{\mathrm{r}}} + \frac{V_{\mathrm{h}}}{T_{\mathrm{h}}} + \frac{V_{\mathrm{e}}}{\gamma T_{\mathrm{he}}}} R_{\mathrm{g}}$	Variation of pressure in the engine
$m_i = \frac{P V_i}{R_g T_i}, (i = c, k, r, h, e)$	Working fluid mass in the engine CVs
$dm_{\mathrm{e}} = \frac{\delta Q_{\mathrm{sh}} + \frac{c_p}{R_g} p dV_e + \frac{c_v}{R_g} V_{\mathrm{e}} dp - c_p T_{\mathrm{ce}} dm_{\mathrm{ce}}}{c_p T_{\mathrm{he}}} + dm_{\mathrm{ce}}$	Change in the mass of working fluid
$dm_{\mathrm{c}} = -\frac{\delta Q_{sh} - \frac{c_p}{R_g} p dV_{\mathrm{c}} - \frac{c_v}{R_g} V_{\mathrm{c}} dp - c_p T_{\mathrm{ce}} dm_{\mathrm{ce}}}{c_p T_{ck}} - dm_{\mathrm{ce}}$	
$dm_i = m_i \frac{dP_i}{P_i}, (i = c, k, r, h, e)$	
$dm_{\mathrm{ck}} = -dm_{\mathrm{c}} - dm_{\mathrm{ce}}$	Interfacial mass flow of engine fluid
$dm_{\mathrm{he}} = dm_{\mathrm{e}} - dm_{\mathrm{ce}}$	
$dm_{\mathrm{kr}} = dm_{\mathrm{ck}} - dm_{\mathrm{k}}$	
$dm_{\mathrm{rh}} = dm_{\mathrm{he}} + dm_{\mathrm{h}}$	
$if\ m_{ck} > 0, T_{ck} = T_k; else\ T_{ck} = T_c$	Conditional temperature variation
$if\ \dot{m}_{\mathrm{ce}} > 0, T_{\mathrm{ce}} = T_{\mathrm{c}}; else, T_{\mathrm{ce}} = T_{\mathrm{e}}$	
$if\ \dot{m}_{\mathrm{kr}} > 0, T_{\mathrm{kr}} = T_{\mathrm{k}}; else, T_{\mathrm{kr}} = T_{\mathrm{k}} + (1 - \varepsilon_{\mathrm{r}})(T_{\mathrm{h}} - T_{\mathrm{k}})$	
$if\ m_{\mathrm{rh}} > 0, T_{\mathrm{rh}} = T_{\mathrm{h}} - (1 - \varepsilon_{\mathrm{r}})(T_{\mathrm{h}} - T_{\mathrm{k}});\ else, T_{\mathrm{rh}} = T_{\mathrm{h}}$	
$if\ m_{he} > 0, T_{he} = T_h; else\ T_{he} = T_e$	
$dT_i = T_i\left(\frac{dV_i}{V_i} + \frac{dP}{P} - \frac{dm_i}{m_i}\right), (i = c, e)$	Variation in temperature in the CVs
$\delta Q_{\mathrm{quasi-ideal,k}} = \frac{c_v}{R_{\mathrm{g}}} V_{\mathrm{k}} dp + c_p\left(T_{\mathrm{ck}}(dm_{\mathrm{c}} + dm_{\mathrm{ce}}) - T_{\mathrm{kr}}(dm_{\mathrm{c}} + dm_{\mathrm{ce}} + dm_{\mathrm{k}})\right)$	Heat lost from cooler
$\delta Q_{\mathrm{quasi-ideal,r}} = \frac{c_v}{R_{\mathrm{g}}} V_{\mathrm{r}} dp + c_p T_{\mathrm{kr}}\left((dm_{\mathrm{c}} + dm_{\mathrm{ce}} + dm_{\mathrm{k}}) - T_{\mathrm{rh}}(dm_{\mathrm{c}} + dm_{\mathrm{ce}} + dm_{\mathrm{k}} + dm_{\mathrm{h}})\right)$	Heat stored in regenerator
$\delta Q_{\mathrm{quasi-ideal,h}} = \frac{c_v}{R_{\mathrm{g}}} V_{\mathrm{h}} dp + c_p\left(T_{\mathrm{rh}}(dm_{\mathrm{c}} + dm_{\mathrm{ce}} + dm_{\mathrm{k}} + dm_{\mathrm{h}}) - T_{\mathrm{he}}(-dm_{\mathrm{e}})\right)$	Heat gained in heater
$\partial W_e = p\, dV_e$	Expansion work done by displacer
$\partial W_c = p\, dV_c$	Compression work done by piston

3.1.1. Heat and work losses in the SE

3.1.1.1. Heat losses

a. Dissipation loss: Some internal energy of the engine fluid is dissipated in the form of heat as it flows through the tubes of the heat exchangers, and this is due to the internal friction. This loss is determined from the pressure drop in the CVs of the engine.

b. Conduction loss: The regenerator wall is maintained at the bulk temperature of the heater and cooler walls. Heat will flow from the walls of the regenerator to the surroundings

because of the temperature difference, and would lead to the loss of the internal energy of the engine fluid.

c. Heat leakage loss to the buffer space: A considerable amount of the engine fluid is lost to the crankcase, as a result of the favourable pressure gradient between the crankcase and the engine cylinder. This will be accompanied by the loss of some useful energy in the engine fluid to the crankcase.

d. Non-ideal heat transfer losses: In the SE, a regenerator is used to minimise the energy added to the engine, by storing some of the internal energy of the engine fluid. In principle, it is expected that all the energy stored in the regenerator will be recovered to fire the engine. However, only a fraction of this energy can be recovered in practice. The amount of energy recovered in the regenerator is defined by its effectiveness; a variable that depends strongly on the geometry and nature of the flow through the regenerator.

3.1.1.2. Work losses

a. Work loss due to pressure drop in the exchangers: The internal walls of the heat exchangers offer some resistance to the free flow of the engine fluid. As a consequence, there will be variations in the pressure of the fluid in these engine components which will lead to work loss. This loss is determined by the flow regime in the heat exchangers of the engine.

b. Loss due to finite speed of the displacer: The pressure of the engine fluid around the displacer during its compression and expansion processes differs from the mean pressure in the engine. Hence, more work is produced in the actual engine during its compression process and less work in the expansion process, leading to loss in the net work.

c. Gas spring loss: When subjected to compressive and expansive forces, the engine's internal gas may begin to act as a spring. Some energy will then be stored in the engine fluid which will be dissipated during its expansion, leading to some loss in the work in the engine.

The losses described so far can be estimated using the following expressions summarised and presented in Table 2.

The actual heat lost by the cooler and added to the heater, respectively are expressed:

$$\dot{Q}_{\mathrm{actual,k}} = \dot{Q}_{\mathrm{quasi-ideal,k}} + \dot{Q}_{\mathrm{cond}} - \dot{Q}_{\mathrm{r,non-ideal}} + \dot{Q}_{\mathrm{leak}} + \dot{Q}_{\mathrm{diss,total}} \quad (5)$$

$$\dot{Q}_{\mathrm{actual,h}} = \dot{Q}_{\mathrm{quasi-ideal,h}} - \dot{Q}_{\mathrm{cond}} + \dot{Q}_{\mathrm{r,non-ideal}} - \dot{Q}_{\mathrm{leak}} - \dot{Q}_{\mathrm{diss,total}} \quad (6)$$

Table 2. Second and third category losses in the non-ideal thermal model with many losses.

Second category (heat) losses	
$Q_{\mathrm{diss,i}} = -\frac{\Delta p_{\mathrm{i}} m_{\mathrm{i}}}{\rho_{\mathrm{g}}}, (i = k, r, h)$	Dissipation loss [28,30]
$Q_{\mathrm{cond}} = R_{\mathrm{cond}}(T_{\mathrm{wh}} - T_{\mathrm{wk}})$	Conduction loss[33]
$Q_{\mathrm{leak}} = m_{\mathrm{leak}} c_p T_{\mathrm{c}}$	Heat leakage loss to the buffer space [27]
$Q_{\mathrm{r,non-ideal}} = Q_{\mathrm{r,ideal}}(1 - \varepsilon_{\mathrm{r}})$	Non-ideal heat loss in the regenerator[27]
$\varepsilon_{\mathrm{r}} = \frac{NTU}{NTU + 1}$	Effectiveness of the regenerator[27]
$NTU = \left(\frac{4Nu}{RePr}\right)\frac{l_{\mathrm{r}}}{d_{\mathrm{hr}}}$	Number of transfer units[34]
$d_{\mathrm{hr}} = \frac{4V_{\mathrm{void,r}}}{A_{\mathrm{wetted,r}}}$	Hydraulic diameter[27]
$Nu = (1 + 0.99(RePr)^{0.66})\phi^{1.79}$	Nusselt number [35]
Third category (work) losses	
$W_{\mathrm{pdrop}} = \oint \sum_{i=k,r,h} \Delta p_{\mathrm{i}}\, dV_{\mathrm{e}}$	Work loss due to pressure drop in the exchangers [28,30]
$\Delta p_{\mathrm{i}} = \frac{2 f_{\mathrm{i}} \mu_{\mathrm{i}} u_{\mathrm{i}} V_{\mathrm{i}}}{d_{\mathrm{hi}}^2 A_{\mathrm{i}}}, (i = k, h, r)$	Pressure drop in the heat exchangers [27]
$f_{\mathrm{i}} = \begin{cases} 16 & Re < 2000 \\ 7.343 \times 10^{-4} Re^{1.3142} & 2000 < Re < 4000 \\ 0.0791 Re^{0.75} & Re > 4000 \end{cases}, (i = k, h)$	Cooler and heater frictional factors [28]
$f_{\mathrm{r}} = 54 + 1.43 Re^{0.78}$	Regenerator frictional factor [36]
$W_{\mathrm{FST\ \&\ mech\ fric}} = \int P_{\mathrm{cylinder}} \left(\pm \frac{\sqrt{3\gamma} u_{\mathrm{p}}}{c} \pm \frac{\Delta p_{\mathrm{f}}}{P_{\mathrm{cylinder}}} \right) dV$	Loss due to finite speed and friction in bearing[37]
$\Delta p_{\mathrm{f}} = 0.97 + 0.15 \frac{N_{\mathrm{r}}}{1000}$	Pressure drop in the bearing[38]
$\dot{W}_{\mathrm{Hyst}} = \sqrt{\frac{1}{32} \omega \gamma^3 (\gamma - 1) T_{\mathrm{w}} p_{\mathrm{mean}} k_{\mathrm{g}} \left(\frac{V_{\mathrm{d}}}{2V_{\mathrm{T}}}\right)^2 A_{wetted}}$	Gas spring loss [28]

On the other hand, the brake power of the engine is obtained from the following expression:

$$\dot{W}_{\mathrm{actual}} = \left\{ \left\{ \oint (p_{\mathrm{e}} dV_{\mathrm{e}} + p_{\mathrm{c}} dV_{\mathrm{c}}) \right\} - W_{\mathrm{FST\ \&\ mech\ fric}} - W_{\mathrm{pdrop}} \right\} Freq - \dot{W}_{\mathrm{Hyst}} \tag{7}$$

Therefore, the SE thermal efficiency is given as:

$$\eta_{\mathrm{Stirling}} = \frac{\dot{W}_{\mathrm{actual}}}{\dot{Q}_{\mathrm{actual,h}}} \tag{8}$$

Please refer to the literature in Ref. [39] and [32] for the expressions and correlations used to update the temperature of the cooler and the heater, at the end of each cycle, and the heat transfer coefficients of the heater and cooler, respectively.

The exergy audit of the SE has been conducted by employing the Second law as presented in [40–42]:

$$\sum_i \dot{Q}\left(1-\frac{T_0}{T}\right)-\sum_o \dot{Q}\left(1-\frac{T_0}{T}\right)-\sum \dot{W}+\sum_i \dot{m}x-\sum_o \dot{m}x = I_{\text{irr}} \qquad (9)$$

In this expression, x, the specific flow exergy is expressed as $x = (h - h_0) - T_0(s - s_0)$.

3.2. Aspen plus modelling of CCHP subsystems

Aspen plus® is a Fortran-based process modelling program that has been extensively used in modelling various processes such as energy systems and refineries. It has a large library of properties of several chemical compounds. In addition, there are custom blocks of commonly used process system components in Aspen plus® which can be easily connected, using materials, heat and work streams [43]. This robust software has been used in the past to model some of the subsystems of the proposed μ-CCHP and the results obtained were comparable to that of other modelling tools, such as the engineering equation solver (EES). Hwang *et al.* [44] reported a relative error of 1.5% in the results obtained from their Aspen model of the lithium bromide/water ARS compared with that from the EES.

In Aspen plus® modelling, the thermophysical properties of the working fluid are determined based on the equation of state; for a pure substance or activity coefficient methods; for non-ideal mixture of solvents [44]. Here, we have used a combination of the Peng-Robinson and the steamNBS as the equation of states to model the conventional components and pure water, respectively. On the other hand, the electrolyte non-random two liquid (ELECNRTL) – an activity coefficient method in Aspen plus® has been used to model the lithium-bromide/water solution. It is also required to define the stream class in Aspen plus® before specifying the streams. In this simulation, we used the MCINCPSD which is compatible with mixed, conventional inert solid with particle size distribution (CIPSD) and non-conventional solids with particle size distribution (NCPSD) streams as the global stream class. The detailed description of the Aspen plus modelling for the various subsystems are undertaken in the following.

3.2.1. Woodchips drying

Here, woodchips drying has been achieved with the aid of the dry reactor (DRY-REAC) and separator (DRY-FLSH) blocks. In the DRY-REAC, some of the volatile components in the woodchips (e.g. moisture) are vaporised with the aid of the high temperature flue. The feedstock is then sent to the DRY-FLSH where the water vapour and the flue are separated from the dry woodchips. These processes require specifying the weight composition of all the

components in the woodchips defined on a dry basis from ultimate and proximate analyses (Table 3). A custom calculator block was deployed to control the moisture composition of the woodchips, at the end of the drying process. This block computes the fractional conversion of woodchips to water which is required to determine the mass flow rate of the woodchips after drying, by conducting a material balance [45]. The final moisture content of the woodchips is set by the user in the calculator block, while the other properties of the wet woodchips are retrieved from the wet woodchips stream.

Table 3. Proximate and Ultimate analyses of white woodchips [47,48].

Composition	Dry Weight (%)
Ultimate analysis	
Hydrogen	6.10
Carbon	51.80
Nitrogen	0.30
Oxygen	41.19
Chlorine	0.00
Sulfur	0.01
Ash	0.60
Moisture	10.00
Proximate analysis	
Moisture	30.00
Fixed Carbon	19.40
Volatile matter	80.00
Ash	0.60

3.2.2. Woodchips combustion

In Aspen plus®, the combustion of solids is achieved in three steps [45]. First, the solid is broken down into its non-stoichiometric components in an Aspen block named RYield (DECOMP). Subsequently, the non-stoichiometric components and the heat of decomposition are admitted into the RGibbs reactor (COMBUSTR). Here, based on the minimisation of the Gibbs free energy, these components will react with air to produce the combustion products. Finally, the combustion products are sent into a solid splitter (SEPARATE) to remove the unburnt solid particles based on a predefined split fraction. To determine the actual composition of the components in the woodchips after the decomposition process, a custom calculator block executed in a Fortran-based environment was deployed. The calculator block accessed the ultimate and proximate analyses of the woodchips in a vector form, based on dry composition from the stream going to the drier. Using the moisture content in the proximate analysis, it converted the ultimate and proximate analyses to a wet basis [45].

352 *3.2.3. ORC modelling*

353 In this study, five Aspen plus® blocks have been used to achieve the ORC modelling,
354 namely, heater (evaporator), expander, solution heat-exchanger, pump and another heat
355 exchanger (condenser). The use of a heater block to implement the evaporator in this design
356 implies that heat is assumed to be added at constant temperature (SE cooler temperature) to
357 the refrigerant of the ORC. Note that the heat input to the heater is supplied from the cooler
358 of the SE implemented in MATLAB by integrating Aspen plus® and MATLAB. The
359 thermodynamic process in the expander was assumed to be polytropic. While a combination
360 of the approach temperature, dryness fraction and discharge pressure have been used to
361 determine the state of the stream at the outlet of the solution heat exchanger, condenser and
362 pump, respectively.

363 Hence, the network output of the ORC and its efficiency is obtained from the following
364 expressions:

$$\dot{W}_{ORC} = \dot{W}_{exp} - \dot{W}_{pump} \tag{10}$$

$$\eta_{ORC} = \frac{\dot{W}_{ORC}}{\dot{Q}_{\text{actual,k}}} \tag{11}$$

365 *3.2.4. ARS modelling*

366 Similar to [44], heater blocks were selected to implement the evaporator, absorber, and
367 condenser of the ARS, on the assumption that heat is added to these components at constant
368 temperature. However, we have harvested the waste heat produced from the absorber and
369 condenser, to improve on the energy efficiency of the DWH. Two pressure reducing valve
370 blocks were used to throttle down the refrigerant (water) and the strong LiBr/water solution
371 to the evaporator pressure. While a pump block that requires only the discharge pressure to be
372 supplied as an input, has been used to lift the weak solution from the absorber to the desorber.
373 To improve the performance of the ARS, a solution heat exchanger (SHX) is usually
374 deployed between the desorber and absorber. The SHX extracts some of the heat from the hot
375 strong solution leaving the desorber to heat up the cold weak solution returning to the
376 desorber, helping to retain the energy in the system. The SHX has been implemented in this
377 design using two heater blocks, where heat is taken from the hot side to the cold side as seen
378 in Fig. 2. Finally, owing to the complexity of the processes in the desorber, a combination of
379 two heaters and a flash separator blocks were selected to implement this process.

380 Thus, the COP of the ARS can be obtained from the given expression:

$$\xi_{ARS} = \frac{\dot{Q}_{evap}}{\dot{Q}_{\text{desorb}} + \dot{W}_{pump}} \quad (12)$$

3.2.5. Domestic water heater modelling

In this CCHP system modelling, the heating of the domestic hot water was implemented in Aspen plus® using a heat-exchanger block. The approach temperature is the only input to the block required to determine the state of the hot water produced. Note that the cold stream input to this block is the water that has been economised in the absorber and condenser of the ARS, while waste heat exiting the desorber of the ARS served as the hot stream inlet to the block.

3.3. CCHP system performance indices

For a power plant comprising several sub-systems and operating simultaneously in close circuit, several performance indicators are required to assess the viability of the plant from thermodynamic, economic and environmental perspectives. While there is no exclusive list of criteria to assess a CCHP plant, some indices have been reported to give deeper insight on the plant's performance. The commonly used performance indicators are those that compare the performance of the CCHP system to that of a conventional SCHP plant [19]. In this study, we have used the energy utilisation factor, exergy efficiency, primary energy saving, artificial thermal efficiency and CO_2 emissions reduction to assess the performance of the μ-CCHP plant from technical, economic and environmental perspectives.

(a) Energy utilisation ratio (EUF):

The EUF assesses the performance of the μ-CCHP plant from the first law perspective. However, because electric power is difficult to produce and highly priced compared with heating or cooling which can be produced with low grade energy and not commensurately priced, EUF is used instead of thermal efficiency. The EUF of a CCHP is expressed as:

$$EUF_{CCHP} = \frac{\dot{W}_{CCHP} + \dot{Q}_{cooling} + \dot{Q}_{heating}}{\dot{m}_{\text{woodchips}} HHV} \quad (13)$$

The net electrical power from the CCHP, $\dot{W}_{CCHP} = \dot{W}_{actual} + \dot{W}_{ORC}$

(b) Exergy efficiency ($\eta_{II,CCHP}$):

Exergy efficiency measures the quality of the energy conversion processes in the CCHP. It is a thermodynamic performance indicator derived from the second law that maps the flow of energy supplied into a system, and reveals where thermodynamic imperfection in a system occurs the most. For a system operating at conditions above the dead state defined by

410 temperature and pressure, $T_o = 298.15\,K$ and $P_o = 101\,kPa$, the exergy efficiency is
411 expressed as:

$$\eta_{II,CCHP} = \frac{\dot{W}_{CCHP} - \left(1 - \frac{T_0}{T_{cooling}}\right)\dot{Q}_{cooling} + \left(1 - \frac{T_0}{T_{heating}}\right)\dot{Q}_{heating}}{\left(1 - \frac{T_0}{T_{flue}}\right)\dot{Q}_{\mathrm{CCHP}}} \tag{14}$$

412 (c) Primary energy saving (PES):

413 Another very insightful way of assessing the performance of a CCHP is by comparing it
414 to the performance of conventional SCHP plants. Herein, we rely on the PES as a preliminary
415 economic indicator, while a comprehensive economic analysis will be conducted in a future
416 work after the optimal system configuration has been obtained. The PES has been widely
417 used by governments to make policies to provide financial support to energy efficient power
418 plants and is a useful and meaningful preliminary economic indicator since it estimates how
419 much fuel is saved in the operation of the system [19]. If the PES is positive, some of the
420 input fuel energy has been saved, while a negative PES value suggests running the plant as a
421 SCHP may be more beneficial. The PES of a CCHP can be obtained from the following
422 expression [2,48]:

$$PES_{CCHP} = 1 - \frac{\dot{Q}_{\mathrm{CCHP}}}{\frac{\dot{W}_{CCHP}}{\eta_{elect,ref}} + \frac{\dot{Q}_{heating}}{\eta_{h,ref}} + \frac{\dot{Q}_{cooling}}{\eta_{h,ref}\xi_{ref}}} \tag{15}$$

423 (d) Artificial thermal efficiency (ATE):

424 If we deduct the energy of the fuel used to produce heating and cooling in a separate
425 boiler of efficiency, η_h and a separate thermal cooler, of COP, ξ_{ref} from the total fuel energy
426 supplied to the CCHP, and divide the electrical power output of the plant by the remaining
427 fuel energy, another performance criterion called the artificial thermal efficiency will be
428 produced. This performance indicator evaluates the efficiency of utilising the fuel to produce
429 electric power in a CCHP system. Therefore, the ATE of a CCHP is expressed as [20]:

$$ATE_{CCHP} = \frac{\dot{W}_{\mathrm{CCHP}}}{\dot{Q}_{CCHP} - \frac{\dot{Q}_{heating}}{\eta_{h,ref}} - \frac{\dot{Q}_{cooling}}{\eta_{h,ref}\xi_{ref}}} \tag{16}$$

430 (e) CO_2 emissions reduction (CO_2ER):

431 An established way of evaluating the performance of a CCHP system is by quantifying its
432 impact on the environment [49]. This can be achieved by comparing the CO_2 emissions
433 reduction of the CCHP system to that of a conventional SCHP system. A positive CO_2ER
434 suggests that the energy system is emitting fewer emissions compared to the SCHP and vice
435 versa. The CO_2ER of the CCHP system can be evaluated from the following expression [6]:

$$CO_2ER_{CCHP} = 1 - \frac{\chi_{CO_2^F}.\dot{Q}_{\text{CCHP}}}{\chi_{CO_2^W}.\dot{W}_{\text{CCHP}} + \frac{\chi_{CO_2^F}.\dot{Q}_{heating}}{\eta_{h,ref}} + \frac{\chi_{CO_2^W}.\dot{Q}_{cooling}}{\eta_{h,ref}\xi_{ref}}} \quad (17)$$

436

437

438 3.4. System integration and solution approach

439 Fig. 5 presents the algorithm for implementing the solutions of the CCHP models in
440 MATLAB and Aspen plus® environment. A code has been developed in the MATLAB
441 environment to interface the SE model with the models built in Aspen plus®. Hence, the
442 control and operation of the CCHP system was achieved in the MATLAB environment.

443

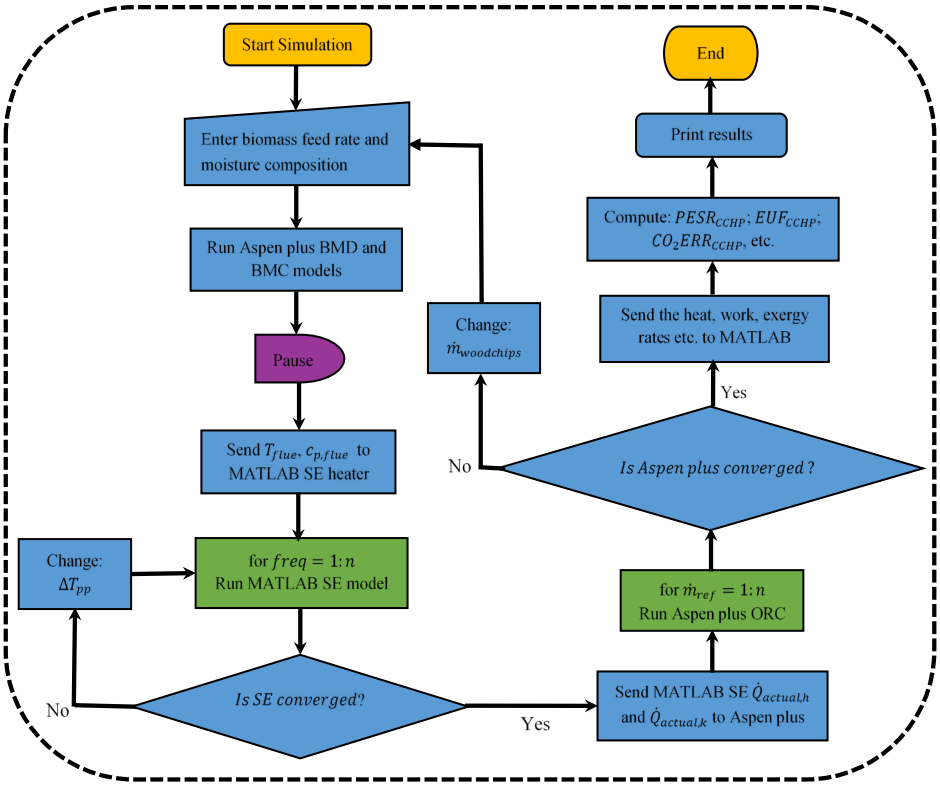

444

445 Fig. 5. Algorithm for the integration of the MATLAB and Aspen plus models of the
446 subsystems of the micro-CCHP.

447 As seen in the algorithm, the woodchips feed rate and required final moisture composition
448 are exported to the respective Aspen plus blocks from MATLAB. The Aspen models of the
449 BMD and BMC are run from MATLAB and the program paused. The temperature and
450 specific heat capacity of the flue produced after the combustion of the woodchips is sent to
451 the SE heater in MATLAB. Using a predefined pinch point temperature, the MATLAB
452 model of the SE is run for a given speed of the engine. The algorithm for solving the
453 governing equations of the SE has been reported in [27]. If the SE model converges, the

results of the energy consumed by the SE heater and that exhausted from the SE cooler are exported to the Aspen plus blocks to implement the Aspen plus models. The Aspen plus program is then run at this point and the steady state solutions of the ORC, ARS and DWH models are obtained. If the program converges, the results of the heat rates, work rates, exergy rates, etc. from these models are returned to MATLAB. Furthermore, these results and that generated for the SE are used to compute the performance indicators of the CCHP. The steps described so far are repeated iteratively for different mass flowrates of the refrigerant flowing through the ARS, so as to achieve different cooling ratios, $CR = \frac{\dot{Q}_{cooling}}{\dot{Q}_{cooling}+\dot{Q}_{heating}}$. Finally, the entire process is repeated for another speed of operation of the prime mover; the SE. Note that if the Aspen plus program does not converge, the woodchips feed rate, $\dot{m}_{woodchips}$ will be changed. The Aspen model may not converge if the flue does not contain sufficient energy to drive some of the subsystems of the CCHP. On the other hand, if the MATLAB SE model does not converge, the pinch point, ΔT_{pp} between the flue and the SE heater temperature is adjusted.

4. Validation of the subsystems of the micro-CCHP

In this section, we present the validation of the SE, ORC and ARS which are subsystems of the micro-CCHP.

4.1. SE validation

The GPU-3 SE designed by General Motors has been extensively reported in the literature for validating the performance of SE models [29]. This 3 kW beta type SE has been deployed to validate the model developed in this study, to predict the experimental data of the SE. The design parameters of the GPU-3 SE are presented in Table 4.

Table 4. Design parameters of GPU – 3 SE [27,29].

Quantity	Value	Quantity	Value
General		Mean tube length	245.30 mm
Working fluid	Helium	Tube outside diameter	4.83 mm
Piston stroke	31.20 mm	Tube inside diameter	3.02 mm
Internal diameter of cylinder	69.90 mm	Number of tubes per cylinder	40.00
Frequency	41.70 Hz	**Cooler**	
Mean Pressure	4.13 MPa	Mean tube length	46.10 mm
Phase angle	90	Tube external diameter	1.59 mm
Heater temperature	977 K	Tube internal diameter	1.09 mm
Cooler temperature	288 K	Number of tubes per cylinder	312.00
Number of cylinder	1	**Volume and clearance**	
Regenerator		Clearance volume of the piston	28.68 mm^3

Regenerator length	226 mm	Clearance volume of the displacer	30.52 mm^3
Regenerator external diameter	80 mm	Dead volume of heater	70.88 mm^3
Regenerator internal diameter	22.60 mm	Dead volume of cooler	13.80 mm^3
Number of regenerator	8	Dead volume of regenerator	50.55 mm^3
Material	Stainless steel wire	Diameter of displacer	69.90 mm
No. of wires per cm	79 × 79	Diameter of displacer rod	9.52 mm
Wire diameter	0.04 mm	Diameter of piston rod	22.20 mm
No of layers	308	Displacer clearance	0.028 mm
Porosity of the regenerator matrix	0.69	Piston clearance	0.15 mm
Heater		Eccentricity	20.80 mm

In this paper, we compare the predicted results of the current model of the SE which was originally developed by the authors in [27] to the experimental data and predicted results of other theoretical models [32,38,50].

Fig. 6 and Fig. 7 that compare the brake power and thermal efficiency of the current model to the aforementioned experimental data and other theoretical model results have been obtained for a SE operating at constant heater and cooler temperatures of 922 K and 286 K, respectively, mean engine pressure of 4.14 MPa and working with helium gas. As seen in Fig. 6, the current model predicted more accurate results of the brake power of the engine than the other models, at all the range of frequencies of the experimental engine investigated except for Li. *et al.* [32] that predicted the brake power of the SE with better accuracy for very low and high frequencies. While in Fig. 7, the current model predicted results of the thermal efficiency of the SE that are consistent with the experimental data, in contrast to the linear trend predicted by the other models.

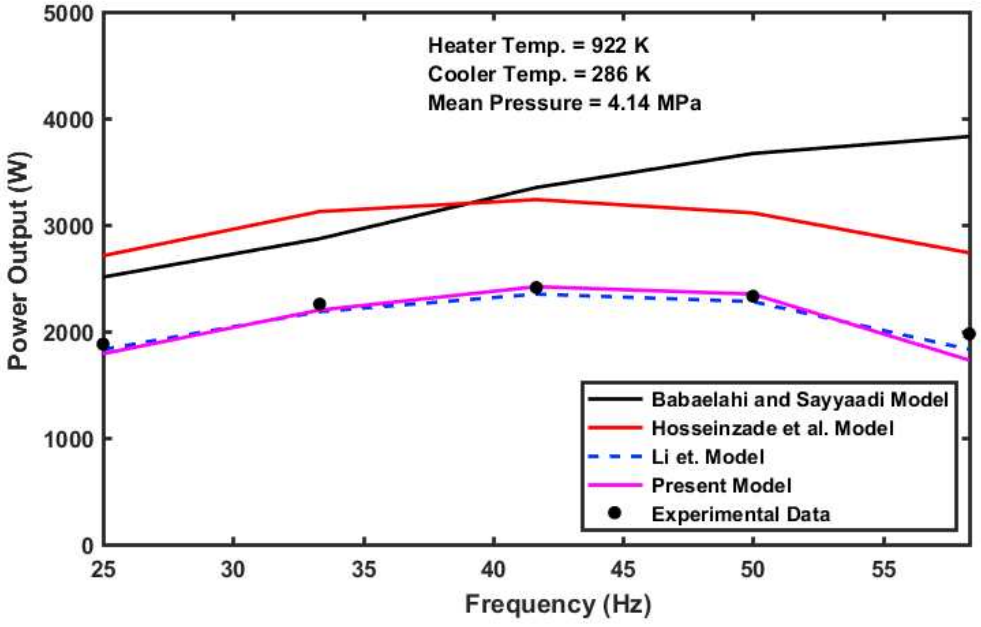

Fig. 6. Validation of the brake power of the SE against experimental data at different speeds.

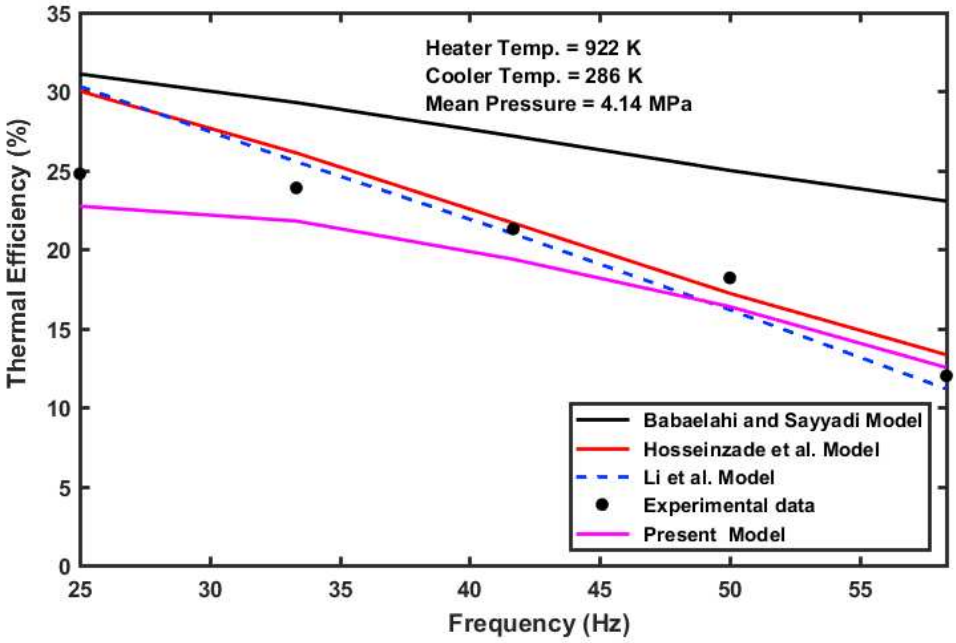

Fig. 7. Validation of thermal efficiency of the Stirling engine at various speeds.

Furthermore, Fig. 8 presents the relative errors in the brake power and energetic efficiency predicted by the current model. As seen in Fig. 8, the relative error in the predicted results remained below 5% for all the speeds of operation of the engine investigated with the exemption of the brake power where the model recorded high relative error for engine frequencies above 50 Hz. The current model has demonstrated a high level of accuracy in predicting the dynamic performance of the experimental engine and is therefore, suitable for the study undertaken in this paper.

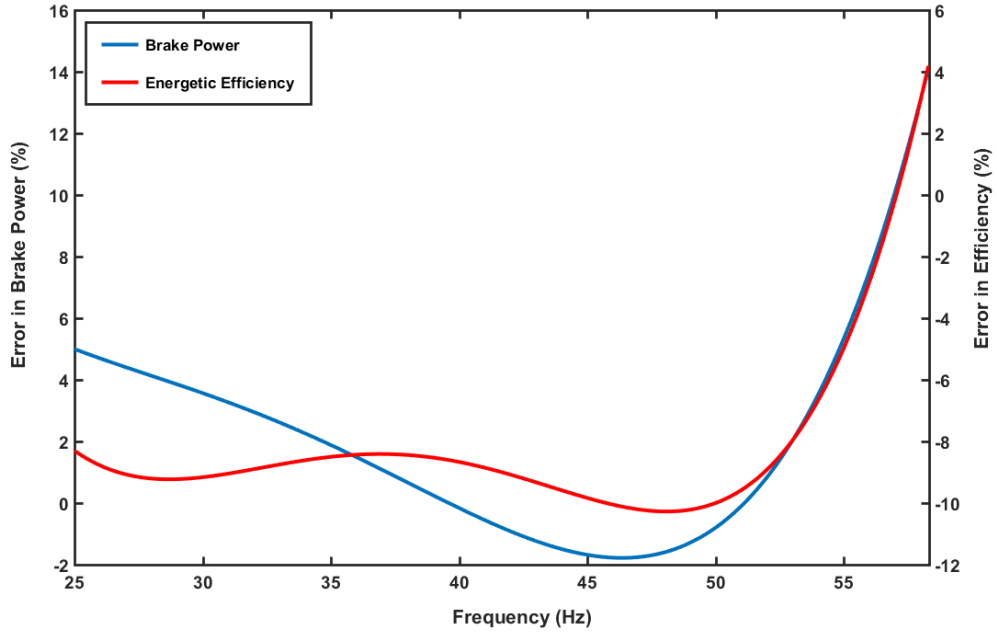

Fig. 8. Prediction error of the SE engine model deployed in this study.

4.2. ORC validation

The model for the prediction of the performance of the ORC engine has been implemented in Aspen plus®. We validated the accuracy of the model using experimental data [41] from a laboratory scale micro-ORC utilising a scroll expander. Table 5 presents the comparison between the Aspen ORC model results and the experimental data, while Table 6 is the operating parameter of the experimental engine. As seen in Table 5, the model predicted results agree remarkably with the experimental data and the maximum relative error recorded in the deviation is 6.43%.

Table 5. Validation of the Aspen plus ORC model against experimental data.

Quantity	Unit	Model result	Experimental result	Relative error (%)
Net power	W	1037	980	5.80
Heat added	W	10441	10500	-0.56
Efficiency	%	9.930	9.330	6.43
Refrigerant flow	kg/s	0.045	0.045	0.00
Pressure ratio	-	4.760	4.760	0.00

Table 6. Flow properties of the experimental ORC engine [41].

Stream	Fluid	State	T (℃)	$P\ (kPa)$	$\dot{m}\ (kg/s)$
12	R245fa	Vapour	89.54	1000.0	0.045
13	R245fa	Vapour	53	210.0	0.045
15	R245fa	Liquid	35	210.0	0.045
11	R245fa	Liquid	36	1000.0	0.045
CWI	Cold Water	Liquid	26	195.0	0.580
CWO	Cold Water	Liquid	32	195.0	0.580
c	Hot Water	Compressed	121	205.0	0.445
d	Hot Water	Compressed	113	158.4	0.445

4.3. Validation of single-effect ARS

In this section, the validation of the ARS model developed in Aspen plus® is presented. In a previous study, Somer *et al*. [44] validated their ARS models built in Aspen plus® against results from EES, due to the paucity of experimental data. They remarked that EES model results provide more information than would experimental data. We have adopted a similar approach in validating our model results by comparing it to the model results produced in Somer *et al*. [44]. To ensure consistency, similar operating data of the single effect lithium bromide-water ARS has been used and is presented in Table 7. As seen in Table 8 showing the results obtained from the model and Somer *et al.* [44], the discrepancy between both model results is less than 1% indicating very good agreement between the models.

526 Table 7. Single-effect LiBr/water ARS operating parameters [44].

Stream	Fluid	$x\ (-)$	T (°C)	$P\ (kPa)$	$\dot{m}\ (kg/s)$	ξ_{LiBr} (%)
17	LiBr/H_2O	0	32.7	0.672	1	57.4
18	LiBr/H_2O	0	32.7	7.461	1	57.4
19	LiBr/H_2O	0	89.9	7.461	1	57.4
20	LiBr/H_2O	0	63.8	7.461	0.918	62.6
21	LiBr/H_2O	0	53.3	7.461	0.918	62.6
22	LiBr/H_2O	0.01	43.1	0.672	0.918	62.6
23	Water	1	78.4	7.461	0.083	0.0
24	Water	0	40.2	7.461	0.083	0.0
25	Water	0.07	1.3	0.672	0.083	0.0
26	water	1	1.3	0.672	0.083	0.0

527

528 Table 8. Results from the Aspen plus model of the ARS.

529
530
531

Quantity	Unit	Model result	Somer *et al.* [44]	Error (%)
$\dot{Q}_{evap}$	W	10764	10772	0.071
$\dot{Q}_{desorb}$	W	14665	14592	-0.500
$\dot{Q}_{abs}$	W	14000	13923	-0.552
$\dot{Q}_{cond}$	W	11429	11432	0.008
ξ_{ARS}	-	0.7330	0.738	0.670

532 ## 5. Results and discussion

533 Here, the impact of retrofitting the SE with an ORC on the power output and thermal
534 efficiency is assessed and compared with a standalone SE for a range of speeds of the prime
535 mover. Furthermore, a detailed sensitivity analysis has been conducted on the effect of
536 cooling ratio and woodchips composition on the dynamic performance of the proposed
537 micro-CCHP.

538 ### 5.1. Standalone SE versus hybrid SE and ORC

539 We compare the performance of the standalone SE to that of a hybrid SE and ORC over a
540 range of operational speeds of the SE prime mover. Fig. 9 presents the power output of SE
541 and ORC only and SE+ORC as well as the thermal efficiency of the combined cycle over a
542 range of speeds of the topping cycle; the SE.

543 It is seen that the power output from the combined cycle nearly doubled for most of the
544 speeds investigated compared with that of the standalone SE. The power output from the SE
545 increases as the speed of the engine increases. However, a decrease in the power output with
546 the increase in speed is observed at very high engine speeds which are characterised by an
547 increase in the losses in the engine. Similarly, the power output from the SE+ORC combined
548 power configuration increases appreciably with the increase in the speed of the SE, and
549 slightly declines at high speeds of the prime mover. The reduction in the negative slope of the

power output at high speeds, for the SE+ORC system compared with the SE only can be attributed to the increase in the power output from the ORC, with the increase in the speed of the prime mover. Waste heat rejected by the cooler of the SE increases as its speed increases, and as a consequence, more energy is available to fire the ORC; hence, the observed trend.

Furthermore, the significance of operating a SE+ORC combined power configuration is also evidenced by the stability in the combined efficiency. As seen in Fig. 9, the efficiency of the combined system remained above 27% even at high engine speeds when the losses in the engine were enormous, and was largely above 30% for the rest of the speeds. This is a remarkable improvement compared to between 12.52 – 22.74% efficiency recorded for the range of speed investigated in the standalone SE (Fig. 7). It is therefore worthy of note that retrofitting an ORC to a SE can significantly improve the performance of the standalone SE from a technical perspective.

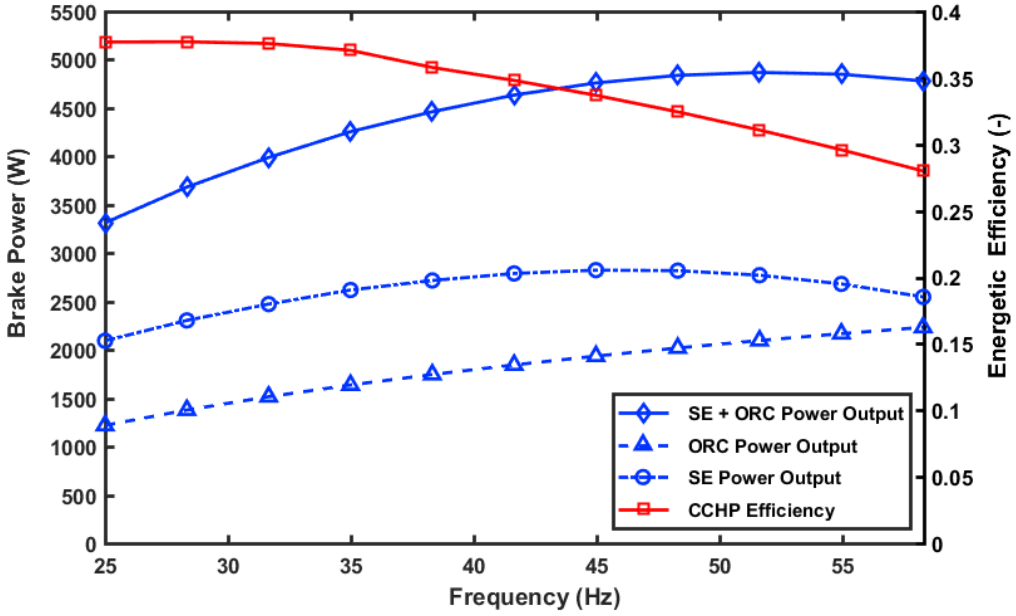

Fig. 9. Assessing the impact of retrofitting a SE with an ORC on the brake power and efficiency of a standalone SE engine.

5.2. Results of sensitivity analysis of the hybrid SE+ORC micro-CCHP

In this section, we present the results for the sensitivity analysis conducted in this study to evaluate the performance of the proposed system from different viewpoints. To this end, we have selected three distinct moisture compositions of the woodchips: 10%, 15% and 20% to represent the likely quality of woodchips in the remote tropical locations as the climatic conditions change. This is intended to investigate the effect of the quality of the input fuel on the plant's performance. Further, on considering the energy requirement for the cooling and heating systems, a sensitivity analysis on the impact of the variation in the cooling and

heating capacities of the CCHP on its performance has also been conducted. This will provide insights into the sizing of the proposed micro-CCHP system as it relates the mix of the energy vectors it should produce to guarantee optimal performance. The performance indicators deployed for the sensitivity analysis were formulated based on thermodynamic, economic and environmental perspectives with the help of the expressions presented in Section 3.3. Table 9 presents the parameters of the reference conventional standalone plant used to evaluate these performance indicators.

Table 9. Input parameters for CCHP performance evaluation.

Parameter	Value	Unit
$\eta_{h,ref}$ [48]	85	-
$\eta_{elect,ref}$ [48]	0.23	-
$\chi_{CO_2^F}$ [51]	220	g (kWh)$^{-1}$
$\chi_{CO_2^W}$ [6]	836	g (kWh)$^{-1}$
ξ_{ref} [48]	3.0	-
*$HHV_{woodchips}$ [47,48]	19220	kJ/kg
$\eta_{m,pump}$	0.67	-
$\eta_{m,exp}$	0.95	-
$\eta_{poly,exp}$	0.87	-
$\eta_{t,pump}$	0.8	-

*The high heating value of woodchips ($HHV_{woodchips}$) is given on a dry basis.

5.2.1. Impact of cooling ratio on μ-CCHP EUF

Fig. 10 (a), (b) and (c) present the effect of cooling ratio on the energy utilization efficiency (EUF_{CCHP}) of the proposed μ-CCHP in a 3-D plot, when fired with woodchips of different moisture compositions for a range of rotational speeds of the prime mover.

It is seen that the ratio of the cooling to heating loads has strong impact on the EUF_{CCHP} of the system. This impact is more severe when the SE prime mover is operating at a low speed. The EUF_{CCHP} declines remarkably as the CR increases, although the decline in EUF_{CCHP} is less intense as the cooling ratio tends to unity [20]. This implies that, the energy in the fuel is better utilised in producing some useful energy in the form of hot water, than in producing cooling. The high efficiency of the hot water boiler compared with the low COP of the single effect ARS may be responsible for the observed trend.

Meanwhile, when the μ-CCHP is producing more heating compared to cooling ($CR < 0.5$), the EUF_{CCHP} decreases with an increase in the speed of the prime mover. At low speed, the μ-CCHP utilises only a small proportion of the energy in the fuel to produce power,

596 making the unused energy available for high efficient hot water heating in the boiler.
597 However, as the speed increases, the SE will start to consume more energy, because of the
598 increase in the losses in the engine; hence, the decline in the EUF_{CCHP}. By contrast, for $CR >$
599 0.5, the EUF_{CCHP} increases, peaks at the mid-speed of about 41.67 Hz ($N = 2500\,rpm$) and
600 starts to decrease. This behavior of the EUF_{CCHP} with an increase in the speed of the SE
601 prime mover for $CR > 0.5$ vary with the moisture content in the woodchips.

602 Thus, in Fig. 10 (a) representing dry woodchips moisture composition of 10%, the
603 EUF_{CCHP} slightly increases as the speed of the engine is increasing and plateaus at high
604 speed. This is because the sufficiently dry woodchips supplies more energy to the combined
605 power system, which enables it to generate significantly higher power than cooling. As a
606 consequence, the EUF_{CCHP} is influenced more by the combined power output, as seen in Eq.
607 (13), resulting to a trend similar to the μ-CCHP power output in Fig. 10. In all, higher
608 EUF_{CCHP} is achieved when using fuel that contains lower moisture to fire the proposed
609 energy system in spite of the cooling ratio and speed of the prime mover.

610

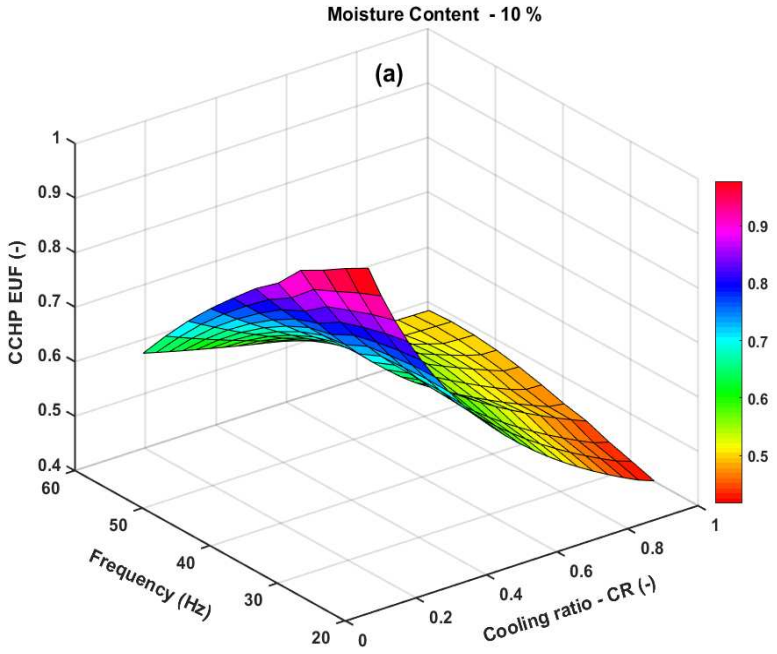

611

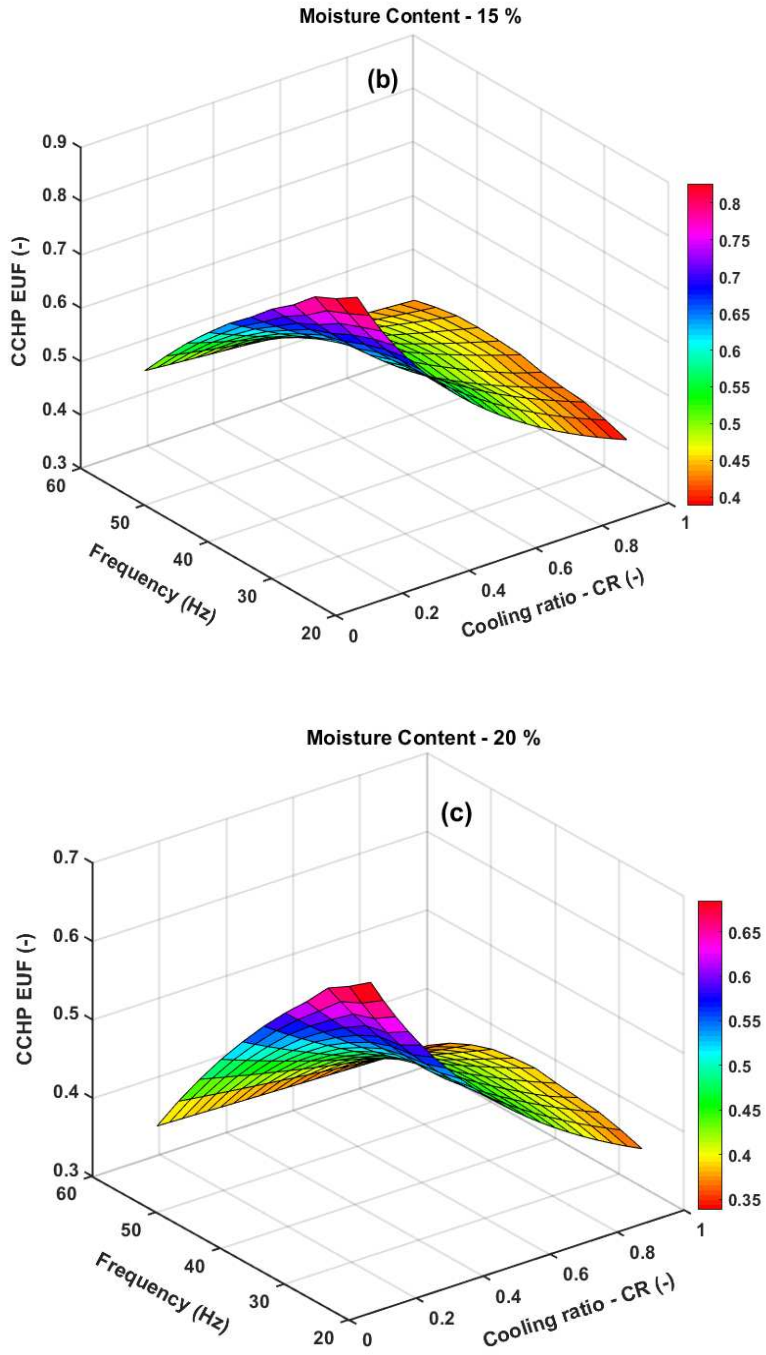

Fig. 10. Evaluating the impact of cooling ratio on the EUF of SE fired μ-CCHP using woodchips of (a) 10% (b) 15% and (c) 20% moisture compositions.

5.2.2. Impact of cooling ratio on μ-CCHP Exergy Efficiency

Fig. 11 (a), (b) and (c) show the impact of cooling ratio and rotational speed of the prime mover on the exergy efficiency ($\eta_{\mathrm{II,CCHP}}$) of the proposed μ-CCHP on a surface plot when fired with woodchips of different moisture compositions.

As seen in Fig. 11, $\eta_{\mathrm{II,CCHP}}$ decreases with increase in cooling ratio, although this decrease is more evident when the woodchips is supplying more energy, *i.e.* contains less

623 moisture. While $\eta_{\mathrm{II,CCHP}}$ increases with increase in the speed of the SE, but flattens out at
624 high rotational speeds and for very low CRs when the energy system is producing more
625 heating. This is the case since the energy conversion process in heating is very efficient;
626 hence, yielding higher $\eta_{\mathrm{II,CCHP}}$. Conversely, low grade energy is usually required to produce
627 cooling in the ARS. Therefore, at low speed when the combined power plant is generating
628 low power, most of the unspent energy is destroyed in the stack resulting to lower second law
629 efficiencies ($\eta_{\mathrm{II,CCHP}}$). However, $\eta_{\mathrm{II,CCHP}}$ significantly improves as more power is produced
630 with increase in the speed of the SE prime mover.

631 Further, the high variation in $\eta_{\mathrm{II,CCHP}}$ between the global optima ($CR = 0.1$ and $freq =$
632 $41.67\ Hz$) and the local optima ($CR = 0.99$ and $freq = 25\ Hz$) from 71% to 20% when
633 using wood chips with 10% moisture content (Fig. 11 (a)) suggests that exergy destruction is
634 more intense in this scenario because the plant is being run at higher temperatures. Hence, it
635 is important to operate the plant within the optimum conditions of the cooling ratio and
636 rotational speed, in order to fully utilise the available energy and enhance efficiency.
637

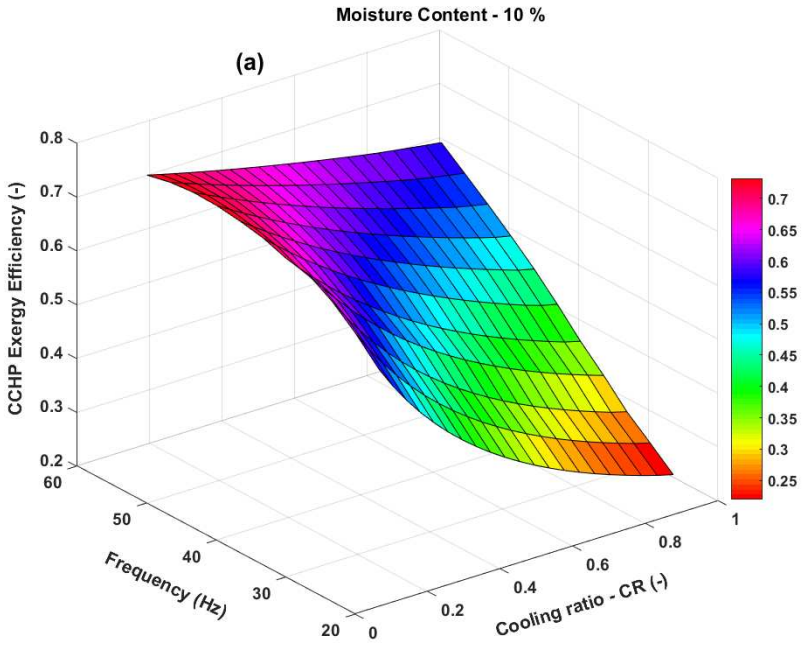

638
639
640
641

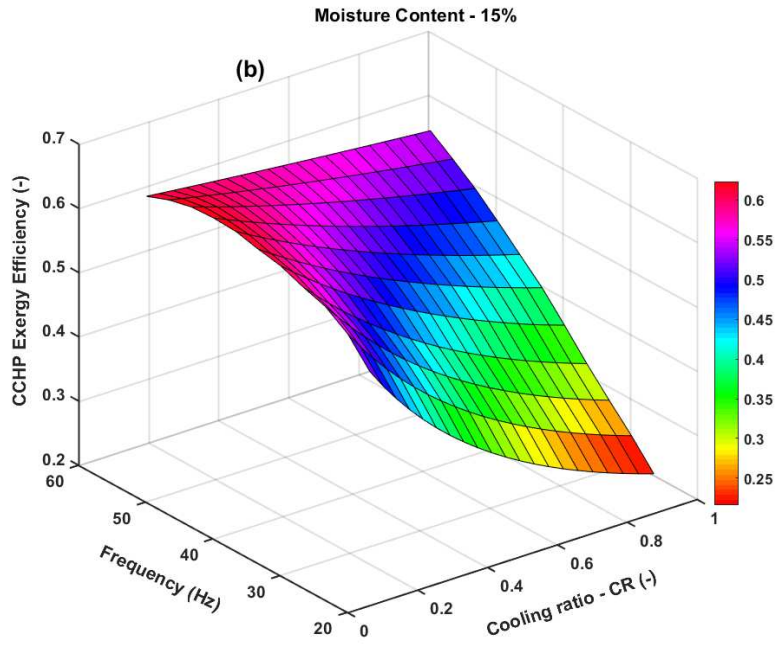

642

643

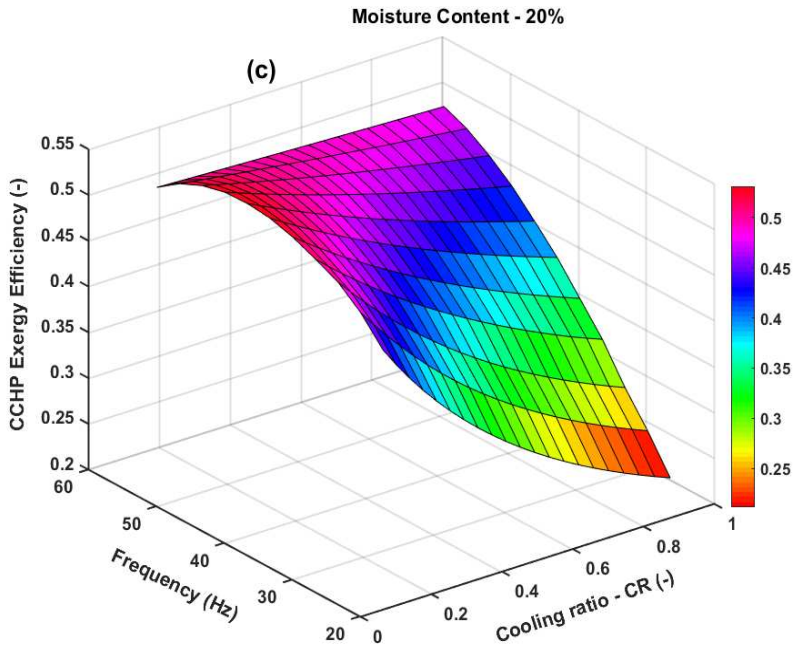

644

645 Fig. 11. Evaluating the impact of cooling ratio on the exergy efficiency of SE fired μ-CCHP
646 using woodchips of (a) 10% (b) 15% and (c) 20% moisture compositions.

647 *5.2.3. Cooling ratio impact on CCHP PES*

648 Fig. 12 (a), (b) and (c) are the surface plots depicting the combined influence of cooling
649 ratio and the rotational speed of the prime mover on the primary energy savings (PES_{CCHP})
650 when woodchips of different moisture composition is deployed to fire the system. As defined
651 in Section 3.3, the PES_{CCHP} compares the energy consumption of the μ-CCHP to that of a
652 SCHP.

653 It is seen that for $CR < 0.25$ (significantly more heating than cooling), the PES_{CCHP}
654 increases with the speed of the prime mover, peaks and decreases slightly [11,13]. This
655 behavior is expected, given that the losses in the SE increases with increase in speed, which
656 makes less energy available for heating water. However, as the CR tends to unity, the
657 PES_{CCHP} simply increases, peaks and plateaus as the speed is increasing. Because the ratio of
658 the power to cooling being produced is high and it has been shown that retrofitting SE with
659 ORC helps to minimise the deterioration in performance at high rotational speeds, the impact
660 of the increasing losses on the PES_{CCHP} is not significant; hence, the observed trend for $CR >$
661 0.25 .

662 Meanwhile, very low and even negative PES_{CCHP} is seen when the μ-CCHP is producing
663 more cooling than heating and the prime mover is operating at low speeds. In particular, for
664 SE operating between frequencies; $25 < freq < 30\ Hz$ ($1500 < N < 1800\ rpm$) and $CR >$
665 0.8, negative PES_{CCHP} is seen in Fig. 12 (b) and (c). Given that at low frequencies and when
666 producing a lot of cooling, the fuel energy supplied to the μ-CCHP is not efficiently utilised
667 to produce power and cooling. Thus, negative PES_{CCHP} is unavoidable in this range of
668 operation of the engine. Therefore, it will be more beneficial to operate the energy system as
669 a SCHP for these ranges of speeds and cooling ratios.

670 Further, over 40% PES_{CCHP} is seen in Fig. 12 (a), for more than 60% of the surface.
671 While in Fig. 12 (b) and (c), it is over 30% and 20% PES_{CCHP}, respectively, for more than
672 60% of the surface. In this regard, the more the energy supplied into the system, the more
673 likely it will be to save energy in a μ-CCHP arrangement where several forms of useful
674 energy are co-produced. This underscores some of the advantages in operating a μ-CCHP
675 configuration compared to conventional SCHP like thermal power plants, where only 30% of
676 the input energy is actually utilised in running the plant. More importantly, from these results,
677 some form of flexibility in the operation and management of the energy system is plausible,
678 since significant primary energy savings is guaranteed over a range of speeds and cooling
679 ratios regardless of the quality of the woodchips fuel.

680

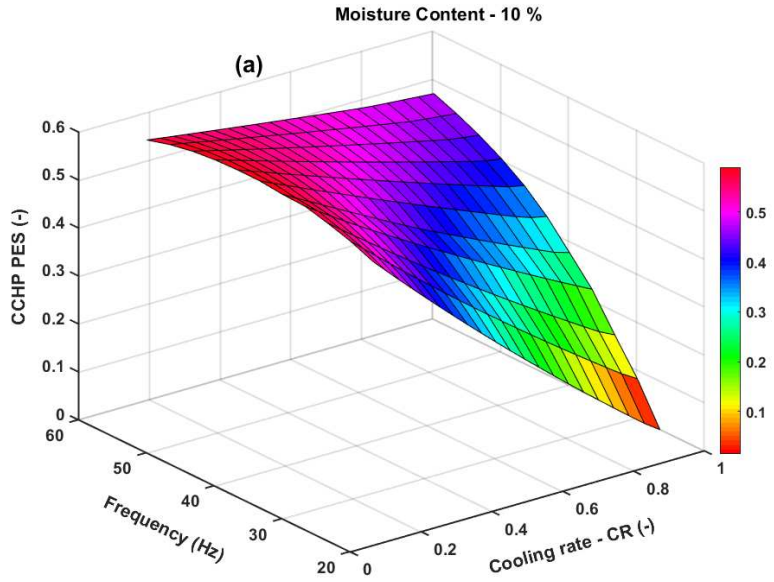

681

682

683

684

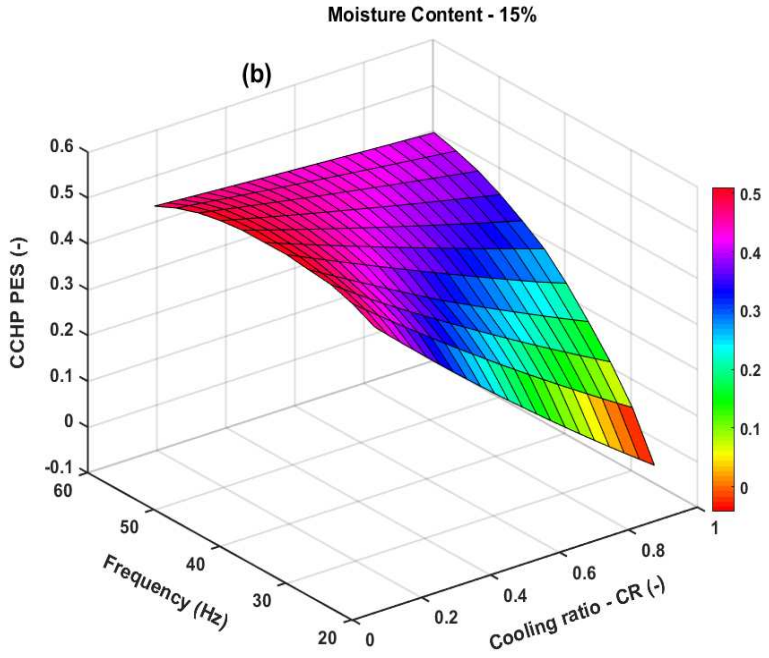

685

686

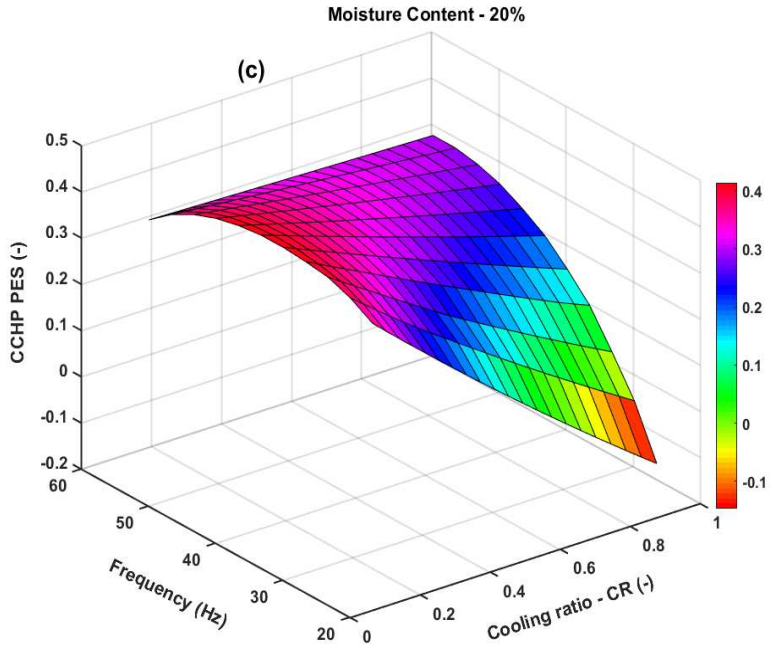

Fig. 12. Evaluating the impact of cooling ratio on the PES of SE fired μ-CCHP using woodchips of (a) 10% (b) 15% and (c) 20% moisture compositions.

5.2.4. Cooling ratio and frequency versus CCHP ATE

Fig. 13 (a), (b) and (c) show the effect of cooling ratio and the rotational speed of the prime mover on the artificial thermal efficiency (ATE_{CCHP}) on a surface plot when woodchips of different moisture composition is deployed to fire the system. In Eq. (16), the ATE_{CCHP} is expressed as the ratio of the power produced by the μ-CCHP and the energy consumed by the energy system with the exclusion of the energy that could have been used to produce cooling and heating, separately.

As seen in Fig. 13, the ATE_{CCHP} decreases with the increase in CR especially at low speed of the prime mover. However, the rate of the decrease in ATE_{CCHP} reduces as the CR tends to 1 [20]. The global optima is seen in a region on the surface plots defined by $freq < 45\,Hz$, and $CR < 0.4$, although the area covered by the global optima reduces and drifts towards lower speed regions as the input fuel quality improves. At low rotational speed of the SE and low CR, when the system is producing more heating than cooling, only a small proportion of the energy supplied to the μ-CCHP is utilised to produce power. As a consequence, high ATE_{CCHP} is seen as expected from the denominator of Eq. (16), suggesting that the energy supplied has been efficiently utilised to produce power.

Further, as the speed of the prime mover increases (beyond $= 30\,Hz$), the ATE_{CCHP} starts to decrease for $CR < 0.4$, due to the increase in the losses in the SE. On the other hand, for $CR > 0.4$, the ATE_{CCHP} increases as the speed of the SE prime mover increases.

Comparing Fig. 13 (a), (b) and (c), the fuel is better utilised to produce power from the μ-CCHP as opposed to producing other forms of useful energy products when the moisture content in the wood chips is low *i.e.* higher input energy. This is seen from the $ATE_{\mathrm{CCHP}} > 30\%$ recorded for over 70% of the surface area in Fig. 13 (a) compared with $ATE_{\mathrm{CCHP}} > 25\%$ and $ATE_{\mathrm{CCHP}} > 20\%$ for over 70% of the surface areas in Fig. 13 (b) and (c), respectively.

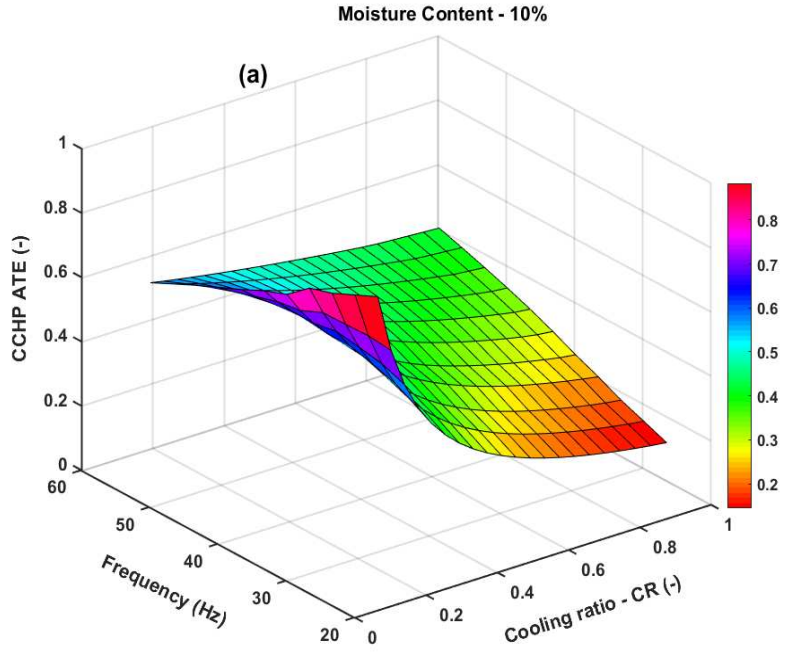

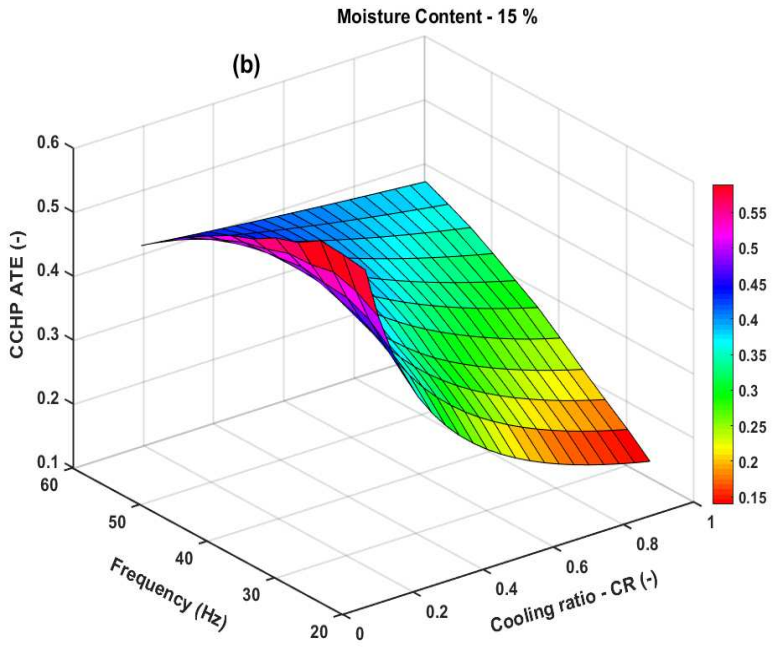

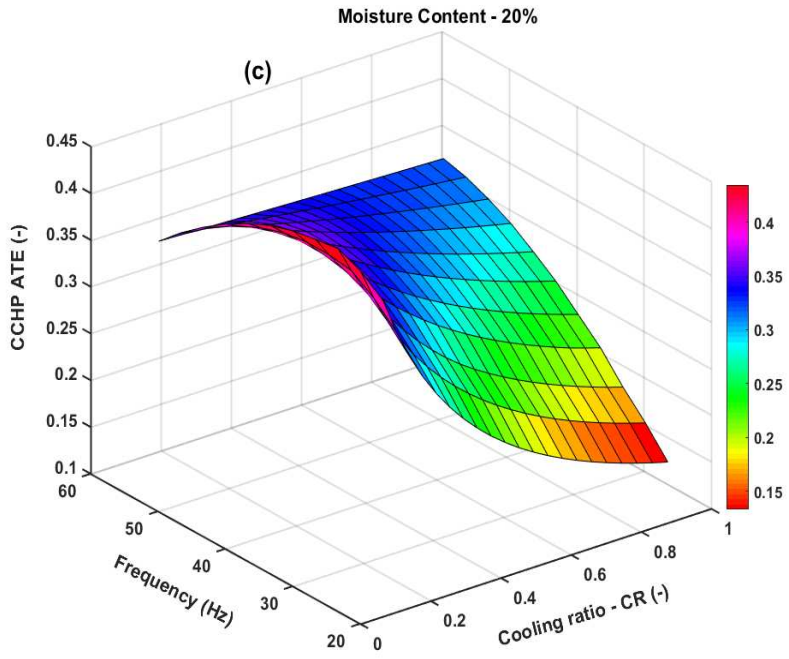

Fig. 13. Evaluating the impact of cooling ratio on the ATE of SE fired μ-CCHP using woodchips of (a) 10% (b) 15% and (c) 20% moisture compositions.

5.2.5. Cooling ratio and frequency versus CCHP CO_2ER

Fig. 14 (a), (b) and (c) compare the CO_2 emissions reduction (CO_2ER_{CCHP}) of the proposed μ-CCHP to that of a SCHP for different cooling and heating capacities and rotational speed of the prime mover when woodchips of different moisture composition is deployed to fire the system.

As seen in Fig. 14, the CO_2ER_{CCHP} capability of the energy system declines as the quality of the input fuel declines. Given that with the increase in moisture content, the combustion process becomes more inefficient, this is expected and can be seen from Eq. (17). CO_2 emissions reductions occur in over 80% (Fig. 14 (a)), 70% (Fig. 14 (b)), and 60% (Fig. 14 (c)) of the surface areas for moisture contents of 10%, 15%, and 20%, respectively.

Meanwhile, negative CO_2ER_{CCHP} were localised in a region characterised by low speed of the prime mover and high cooling ratios. Similar to what has been reported in the case of the PES_{CCHP}, the low amount of power being generated by the SE prime mover at low speed is responsible for the observed trend. In addition, when producing a lot of cooling, only a fraction of the energy supplied to the µ-CCHP is utilised by the thermal chiller. The rest obviously will end in the environment as exhaust gas. Thus, it is expected that a conventional SCHP would reduce CO_2 emissions better, when operating in these regimes.

741 Generally, as more cooling is being produced relative to heating, CO_2ER_{CCHP} declines
742 because of the lower energy conversion efficiency in cooling compared to heating. On the
743 other hand, CO_2ER_{CCHP} increases with the increase in the rotational speed of the prime mover
744 and slightly declines at very high speed for the case of $CR < 0.2$ and with high moisture in
745 the fuel. Finally, up to 43%, 40%, and 31% reductions in CO_2 emissions can be achieved
746 using woodchips of 10% (Fig. 14 (a)), 15% (Fig. 14 (b)) and 20% (Fig. 14 (c)) moisture
747 contents, respectively.

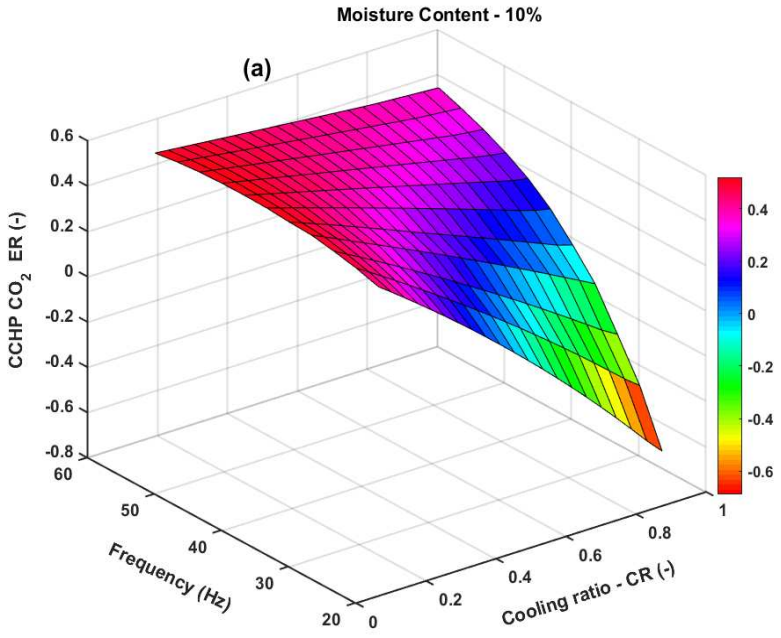

748
749

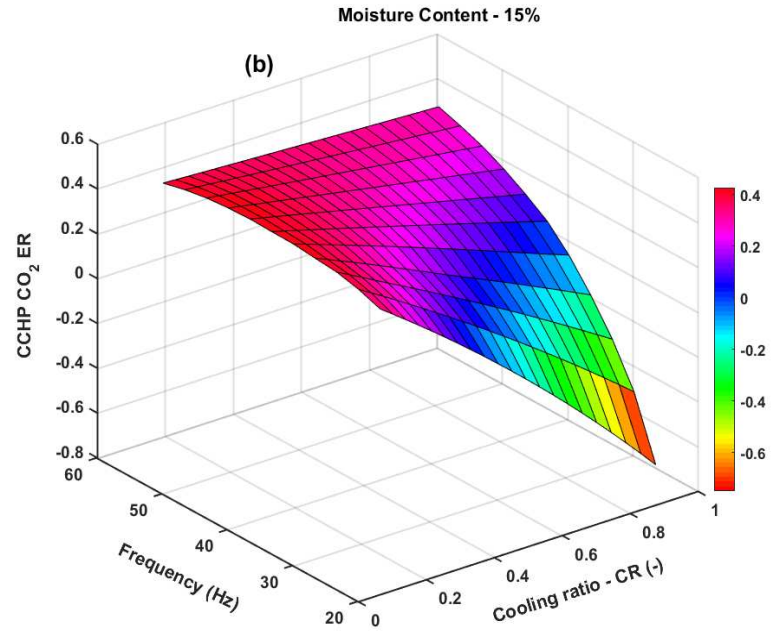

750

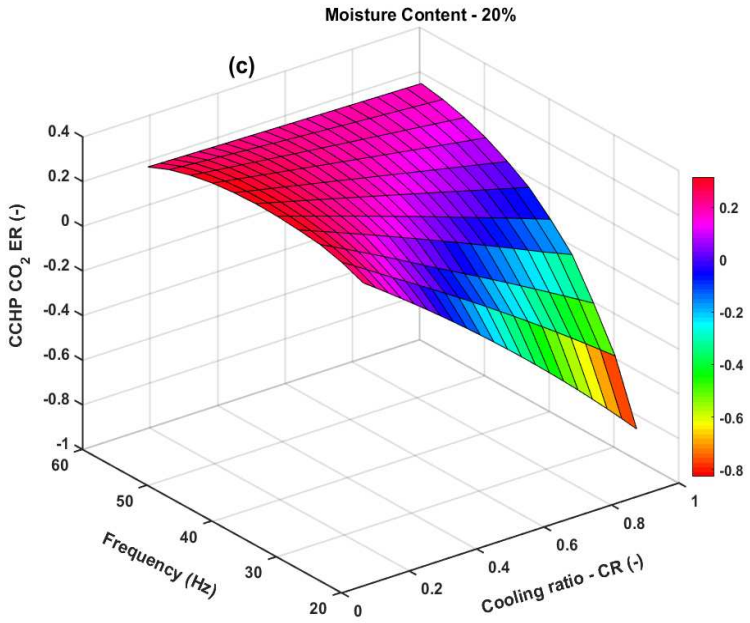

Fig. 14. Evaluating the impact of cooling ratio on the CO_2ER of SE fired μ-CCHP using woodchips of (a) 10% (b) 15% and (c) 20% moisture compositions.

5.3. Discussions

In a broad sense, it is seen that deploying a hybrid of the Stirling engine and ORC as prime movers in the proposed micro-CCHP system design minimised the losses in the system and improved its performance indicators. In particular, compared to previous studies, the steep decline in PES_{CCHP} at high speed of the SE prime mover has been significantly reduced in this study. This is because the waste heat which is rejected in other studies has been utilised to produce additional power in the ORC. A maximum of 55% savings in the primary energy is recorded when the system is fired by biomass fuel with 10% moisture content, producing more heating load, and operating at a rotational speed of 2500 rpm compared to a PES_{CCHP} of 24.05%, 29.47% and 42% recorded in Ref. [10], [11] and [13], respectively. Similarly, higher CO_2ER_{CCHP} are also seen here compared with some previous studies. In this study, a maximum CO_2ER_{CCHP} of 45% is recorded when biomass fuel with 10% moisture is deployed to produce a significant amount of heating and power at rotational speeds above 2000 rpm. This is more than the CO_2ER_{CCHP} of 31.06%, and 36.22% obtained in the CCHP designs in Ref. [10] and [11], respectively, that utilised SE only as the prime mover, but slightly lower than 46.6% reported in Ref. [13] where a hybrid of the IC engine and SE was deployed. This underscores the gains in using hybrid prime movers in micro-CCHP systems.

Further, the ratio of the cooling load to the heating load that the system is designed to meet has a significant impact on its performance. This impact is seen to be very severe in the

PES_{CCHP} and CO_2ER_{CCHP} where negative values were recorded especially when the system was fired with fuel of high moisture content. It is seen that the micro-CCHP performed creditably when it serviced more of the heating load and power compared with the cooling load and power and this is similar to the findings in Ref. [20]. There is an obvious need to size the system to determine how much cooling or heating it should service.

Also, in-situ drying of the woodchips fuel is promising and has ensured that the quality of the input fuel is maintained at all seasons. The maximum values of PES_{CCHP}, $\eta_{\mathrm{II,CCHP}}$, EUF_{CCHP}, ATE_{CCHP} and CO_2ER_{CCHP} recorded for 10%, 15% and 20% moisture composition of woodchips fuel are: 55%, 71%, 94%, 85%, 43%; 50%, 61%, 81%, 60%, 40%; and 40%, 53%. 67%, 45%, 31%, respectively. The quality of the biomass fuel is seen to have impacted on the system's performance metrics, particularly the EUF and ATE, where a significant change is observed as the moisture content of the fuel increases.

6. Conclusion

In this paper, a novel micro-CCHP (μ-CCHP) system that hybridises a Stirling engine (SE) and an ORC was designed and assessed; to co-produce power, cooling from an absorption chiller (ARS) and domestic hot water from a boiler (DWH). By calculating typical techno-enviro-economic indicators, such as primary energy saving, energy utilisation factor, exergy efficiency, artificial thermal efficiency and CO_2 emissions reduction, the performance of the μ-CCHP has been evaluated. The influence of rotational speed of the prime mover, cooling and heating capacities and quality of biomass fuel on the performance of the μ-CCHP have been assessed and compared with conventional separate cooling, heating and power (SCHP) systems. The key findings of this study are itemised in the following:

- An increase in the rotational speed of the SE led to the increase in the heat sink temperature and a consequent increase in the power output from the ORC. Hybridising SE with ORC increases the power output of a standalone SE by a minimum of 55% at all the rotational speeds investigated.
- A mild decline in the thermal efficiency of the hybrid SE+ORC with high rotational speeds is observed contrary to the steep decline in SE only systems. At the rotational speed of 1500 rpm, maximum efficiency of 37% was recorded for the hybrid SE and ORC compared to 22.74% recorded for the standalone SE.
- PES_{CCHP} is largely positive for $CR < 0.5$ when the μ-CCHP was servicing more heating load than cooling load in conjunction with the power demand. Maximum PES_{CCHP} of

40%, 50% and 55% were obtained at medium speed and very low CR, for 20%, 15%, and 10% dry woodchips, respectively.

- An increase in CR led to significant decrease in the ATE_{CCHP}, although the value starts to converge as the CR tends to one, evident at low operational speed. Maximum ATE_{CCHP} are obtained as seen in the global optima for a range of frequencies of 25 – 30 Hz, 25 – 40 Hz, and 35 - 45 Hz, using 10%, 15% and 20% dry woodchips fuel, respectively.
- A decrease in CO_2ER_{CCHP} with an increase in CR is observed with an increased intensity at low rotational speed of the prime mover. Maximum CO_2ER_{CCHP} of 43%, 40%, and 31% were obtained in the μ-CCHP compared with SCHP when using woodchips fuel that contains 10%, 15%, 20% moisture, respectively, to fire the system.
- Negative PES_{CCHP} and CO_2ER_{CCHP} are obtained in regions defined by very low rotational speeds and high CRs, *i.e.* when the μ-CCHP is producing more cooling and low power, suggesting that the fuel is being underutilised.
- ATE_{CCHP} and EUF_{CCHP} were impacted more by the change in the moisture content in the fuel and recorded between 13% to 25% decline with the increase in moisture content of the fuel.

This study has provided new insights into the role hybridising SE and ORC, cooling ratio, and quality of woodchips fuel play in the performance of the proposed system. The conclusions here favour the sizing optimisation of the proposed μ-CCHP system to determine its optimal configuration before deployment in remote off-grid locations, where access to electricity is limited, to provide electricity and other energy vectors, such as heating and cooling, to preserve and process their agricultural produce.

Acknowledgements

This study was funded by the Petroleum Technology Development Fund, an agency of the Ministry of Petroleum Resources, in Nigeria.

References

[1] Ebrahimi M, Keshavarz A. Combined Cooling, Heating and Power Decision-making, Design and Optimisation. First edit. Elsevier Ltd; 2015.

[2] Piacentino A, Barbaro C, Cardona F, Gallea R, Cardona E. A comprehensive tool for efficient design and operation of polygeneration-based energy μgrids serving a cluster of buildings. Part I: Description of the method. Appl Energy 2013;111:1204–21. doi:10.1016/j.apenergy.2012.11.078.

837 [3] Renzi M, Brandoni C. Study and application of a regenerative Stirling cogeneration
838 device based on biomass combustion. Appl Therm Eng 2014;67:341–51.
839 doi:10.1016/j.applthermaleng.2014.03.045.
840 [4] Ebrahimi M, Keshavarz A. Sizing the prime mover of a residential micro-combined
841 cooling heating and power (CCHP) system by multi-criteria sizing method for
842 different climates. Energy 2013;54:291–301. doi:10.1016/j.energy.2013.01.061.
843 [5] Thiers S, Aoun B, Peuportier B. Experimental characterization, modeling and
844 simulation of a wood pellet micro-combined heat and power unit used as a heat source
845 for a residential building. Energy Build 2010;42:896–903.
846 doi:10.1016/j.enbuild.2009.12.011.
847 [6] Chicco G, Mancarella P. Assessment of the greenhouse gas emissions from
848 cogeneration and trigeneration systems. Part I: Models and indicators. Energy
849 2008;33:410–7. doi:10.1016/j.energy.2007.10.006.
850 [7] Bocci E, Sisinni M, Moneti M, Vecchione L, Di Carlo A, Villarini M. State of art of
851 small scale biomass gasification power systems: A review of the different typologies.
852 Energy Procedia 2014;45:247–56. doi:10.1016/j.egypro.2014.01.027.
853 [8] González-Pino I, Campos-Celador A, Pérez-Iribarren E, Terés-Zubiaga J, Sala JM.
854 Parametric study of the operational and economic feasibility of Stirling micro-
855 cogeneration devices in Spain. Appl Therm Eng 2014;71:821–9.
856 doi:10.1016/j.applthermaleng.2013.12.020.
857 [9] González A, Riba JR, Puig R, Navarro P. Review of micro- and small-scale
858 technologies to produce electricity and heat from Mediterranean forests' wood chips.
859 Renew Sustain Energy Rev 2015;43:143–55. doi:10.1016/j.rser.2014.11.013.
860 [10] Chahartaghi M, Sheykhi M. Energy, environmental and economic evaluations of a
861 CCHP system driven by Stirling engine with helium and hydrogen as working gases.
862 Energy 2019;174:1251–66. doi:10.1016/j.energy.2019.03.012.
863 [11] Sheykhi M, Chahartaghi M, Balakheli MM, Kharkeshi BA, Miri SM. Energy, exergy,
864 environmental, and economic modeling of combined cooling, heating and power
865 system with Stirling engine and absorption chiller. Energy Convers Manag 2019.
866 doi:10.1016/j.enconman.2018.10.102.
867 [12] Karami R, Sayyaadi H. Optimal sizing of Stirling-CCHP systems for residential
868 buildings at diverse climatic conditions. Appl Therm Eng 2015;89:377–93.
869 doi:10.1016/j.applthermaleng.2015.06.022.
870 [13] Sheykhi M, Chahartaghi M, Balakheli MM, Hashemian SM, Miri SM, Rafiee N.

871 Performance investigation of a combined heat and power system with internal and
872 external combustion engines. Energy Convers Manag 2019;185:291–303.
873 doi:10.1016/j.enconman.2019.01.116.
874 [14] Bahrami M, Hamidi AA, Porkhial S. Investigation of the effect of organic working
875 fluids on thermodynamic performance of combined cycle Stirling-ORC. Int J Energy
876 Environ Eng 2013;4:1–9.
877 [15] Korlu M, Pirkandi J, Maroufi A. Thermodynamic analysis of a gas turbine cycle
878 equipped with a non-ideal adiabatic model for a double acting Stirling engine. Energy
879 Convers Manag 2017;147:120–34. doi:10.1016/j.enconman.2017.04.049.
880 [16] Entezari A, Manizadeh A, Ahmadi R. Energetical, exergetical and economical
881 optimization analysis of combined power generation system of gas turbine and Stirling
882 engine. Energy Convers Manag 2018;159:189–203.
883 doi:10.1016/j.enconman.2018.01.012.
884 [17] Hosseinpour J, Sadeghi M, Chitsaz A, Ranjbar F, Rosen MA. Exergy assessment and
885 optimization of a cogeneration system based on a solid oxide fuel cell integrated with a
886 Stirling engine. Energy Convers Manag 2017;143:448–58.
887 doi:10.1016/j.enconman.2017.04.021.
888 [18] Ansarinasab H, Mehrpooya M. Investigation of a combined molten carbonate fuel cell,
889 gas turbine and Stirling engine combined cooling heating and power (CCHP) process
890 by exergy cost sensitivity analysis. Energy Convers Manag 2018;165:291–303.
891 doi:10.1016/j.enconman.2018.03.067.
892 [19] Cardona E, Piacentino A. A methodology for sizing a trigeneration plant in
893 mediterranean areas. Appl Therm Eng 2003;23:1665–80. doi:10.1016/S1359-
894 4311(03)00130-3.
895 [20] Maraver D, Sin A, Royo J, Sebastián F. Assessment of CCHP systems based on
896 biomass combustion for small-scale applications through a review of the technology
897 and analysis of energy efficiency parameters. Appl Energy 2013;102:1303–13.
898 doi:10.1016/j.apenergy.2012.07.012.
899 [21] Liu W, Chen G, Yan B, Zhou Z, Du H, Zuo J. Hourly operation strategy of a CCHP
900 system with GSHP and thermal energy storage (TES) under variable loads: A case
901 study. Energy Build 2015;93:143–53. doi:10.1016/j.enbuild.2015.02.030.
902 [22] Kaldehi BJ, Keshavarz A, Safaei Pirooz AA, Batooei A, Ebrahimi M. Designing a
903 micro Stirling engine for cleaner production of combined cooling heating and power in
904 residential sector of different climates. J Clean Prod 2017;154:502–16.

905 doi:10.1016/j.jclepro.2017.04.006.
906 [23] Damirchi H, Najafi G, Alizadehnia S, Mamat R, Nor Azwadi CS, Azmi WH, et al.
907 Micro Combined Heat and Power to provide heat and electrical power using biomass
908 and Gamma-type Stirling engine. Appl Therm Eng 2016;103:1460–9.
909 doi:10.1016/j.applthermaleng.2016.04.118.
910 [24] Cardozo E, Malmquist A. Performance comparison between the use of wood and
911 sugarcane bagasse pellets in a Stirling engine micro-CHP system. Appl Therm Eng
912 2019;159:113945. doi:10.1016/j.applthermaleng.2019.113945.
913 [25] Harrod J, Mago PJ. Performance analysis of a combined cooling, heating, and power
914 system driven by a waste biomass fired Stirling engine. Proc Inst Mech Eng Part C J
915 Mech Eng Sci 2011;225:420–8. doi:10.1243/09544062JMES2086.
916 [26] Mustelier NL, Almeida MF, Cavalheiro J, Castro F. Evaluation of pellets produced
917 with undergrowth to be used as biofuel. Waste and Biomass Valorization 2012;3:285–
918 94. doi:10.1007/s12649-012-9127-5.
919 [27] Udeh GT, Michailos S, Ingham D, Hughes KJ, Ma L, Pourkashanian M. A new non-
920 ideal second order thermal model with additional loss effects for simulating beta
921 Stirling engines. Energy Convers Manag 2020;206.
922 doi:10.1016/j.enconman.2020.112493.
923 [28] Urieli I, Berchowitz D. Stirling cyle engine analysis. Adam Hilger LTD 1984.
924 [29] Martini W. Stirling Engine Design Manual Conservation and Renewable Energy.
925 Methods 1983:412.
926 [30] Ã YT, Tlili I, Nasrallah S Ben. Design and performance optimization of GPU-3
927 Stirling engines. Energy 2008;33:1100–14. doi:10.1016/j.energy.2008.02.005.
928 [31] Homutescu VM, Dumitrascu G, Horbaniuc B. Evaluation of the work lost due to leaks
929 through cylinder-displacer gap 2008.
930 [32] Li R, Grosu L, Li W. New polytropic model to predict the performance of beta and
931 gamma type Stirling engine. Energy 2017;128:62–76.
932 doi:10.1016/j.energy.2017.04.001.
933 [33] Araoz JA, Salomon M, Alejo L, Fransson TH. Non-ideal Stirling engine
934 thermodynamic model suitable for the integration into overall energy systems. Appl
935 Therm Eng 2014;73:203–19. doi:10.1016/j.applthermaleng.2014.07.050.
936 [34] Alfarawi S, Al-Dadah R, Mahmoud S. Enhanced thermodynamic modelling of a
937 gamma-type Stirling engine. Appl Therm Eng 2016;106:1380–90.
938 doi:10.1016/j.applthermaleng.2016.06.145.

939 [35] Ahmed F, Hulin H, Khan AM. Numerical modeling and optimization of beta-type
940 Stirling engine. Appl Therm Eng 2019;149:385–400.
941 doi:10.1016/j.applthermaleng.2018.12.003.
942 [36] Kays WM, London AL. Compact Heat Exchangers. Krieger Pub Co.; 1998.
943 [37] Petrescu S, Costea M. Development of thermodynamics with finite speed and direct
944 method. Ed AGIR 2011.
945 [38] Babaelahi M, Sayyaadi H. Simple-II: A new numerical thermal model for predicting
946 thermal performance of Stirling engines. Energy 2014;69:873–90.
947 doi:10.1016/j.energy.2014.03.084.
948 [39] Babaelahi M, Sayyaadi H. A new thermal model based on polytropic numerical
949 simulation of Stirling engines. Appl Energy 2015;141:143–59.
950 doi:10.1016/j.apenergy.2014.12.033.
951 [40] Tchanche BF, Lambrinos G, Frangoudakis A, Papadakis G. Exergy analysis of micro-
952 organic Rankine power cycles for a small scale solar driven reverse osmosis
953 desalination system. Appl Energy 2010;87:1295–306.
954 doi:10.1016/j.apenergy.2009.07.011.
955 [41] Baral S, Kim D, Yun E, Kim KC. Energy, exergy and performance analysis of small-
956 scale organic rankine cycle systems for electrical power generation applicable in rural
957 areas of developing countries. Energies 2015;8:684–713. doi:10.3390/en8020684.
958 [42] Cakici DM, Erdogan A, Colpan CO. Thermodynamic performance assessment of an
959 integrated geothermal powered supercritical regenerative organic Rankine cycle and
960 parabolic trough solar collectors. Energy 2017;120:306–19.
961 doi:10.1016/j.energy.2016.11.083.
962 [43] Ye G, Xie D, Qiao W, Grace JR, Lim CJ. Modeling of fluidized bed membrane
963 reactors for hydrogen production from steam methane reforming with Aspen Plus. Int J
964 Hydrogen Energy 2009;34:4755–62. doi:10.1016/j.ijhydene.2009.03.047.
965 [44] Somers C, Mortazavi A, Hwang Y, Radermacher R, Rodgers P, Al-Hashimi S.
966 Modeling water/lithium bromide absorption chillers in ASPEN Plus. Appl Energy
967 2011;88:4197–205. doi:10.1016/j.apenergy.2011.05.018.
968 [45] Aspen Plus. Getting Started Modeling Processes with Solids Aspen Plus. Toll Free
969 2012. doi:10.1016/S1164-0235(02)00075-4.
970 [46] Dimitriou I, Goldingay H, Bridgwater A V. Techno-economic and uncertainty analysis
971 of Biomass to Liquid (BTL) systems for transport fuel production. Renew Sustain
972 Energy Rev 2018;88:160–75. doi:10.1016/j.rser.2018.02.023.

973 [47] Michailos S, Emenike O, Ingham D, Hughes KJ, Pourkashanian M. Methane
974 production via syngas fermentation within the bio-CCS concept: A techno-economic
975 assessment. Biochem Eng J 2019;150:107290. doi:10.1016/j.bej.2019.107290.
976 [48] Badea N. Design for Micro-Combined Cooling, Heating and Power Systems. Springer
977 Berlin Heidelberg; 2015. doi:10.1007/978-1-4471-6254-4.
978 [49] Foumani M, Smith-Miles K. The impact of various carbon reduction policies on green
979 flowshop scheduling. Appl Energy 2019;249:300–15.
980 doi:10.1016/j.apenergy.2019.04.155.
981 [50] Hosseinzade H, Sayyaadi H, Babaelahi M. A new closed-form analytical thermal
982 model for simulating Stirling engines based on polytropic-finite speed
983 thermodynamics. Energy Convers Manag 2015;90:395–408.
984 doi:10.1016/j.enconman.2014.11.043.
985 [51] Chicco G, Mancarella P. Assessment of the greenhouse gas emissions from
986 cogeneration and trigeneration systems. Part I: Models and indicators. vol. 33. n.d.
987 doi:10.1016/j.energy.2007.10.006.
988

989 ## Nomenclature

General		$elect$	electricity
A	cross sectional area (m^2)	$evap$	evaporator
C_{pg}	Isobaric specific heat of gas(J/kgK)	exp	expansion
CR	cooling ratio ($-$)	f	friction
C_{vg}	Isochoric specific heat of gas (J/kgK)	$flue$	flue gas
d	diameter of component (m)	FST	finite speed thermodynamics
ER	emission reduction	h	heater
f	frictional factor ($-$)	he	heater – hot space
$freq$	engine frequency(Hz)	$hyst$	hysteresis
h	heat transfer coefficient ($W/m^2\,K$)	irr	irriversibility
HHV	high heating value (J/kg)	k	cooler
I	exergy destruction rate (W)	kr	cooler – regenerator
J	displacer gap (m)	$leak$	crankcase
k	thermal conductivity (W/mK)	$mech\ fric$	mechanical friction
L	length of component (m)	m	mechanical

m	mass of gas (kg)	o	dead state
NTU	number of transfer units $(-)$	$pdrop$	pressure drop
Nu	Nusselt number $(-)$	$poly$	polytropic
P	pressure (Pa)	pp	pinch point
Pr	Prandtl number $(-)$	r	regenerator
Q	heat added or lost (J)	ref	reference
Re	Reynold number $(-)$	rh	regenerator - heater
R_g	gas constant (J/kgK)	sh	shuttle
s	specific entropy (J/kgK)	t	transmission
T	temperature (K)	w	wall
u	gas velocity (m/s)	**Superscript**	
V	volume (m^3)	F	fuel
W	work output (J)	W	network electricity
x	flow exergy (J/kg)	**Greek**	
Z	displacer stoke (m)	γ	isentropic exponent $(-)$
Subscript		χ	emission factor (gW/s)
c	cold space	ρ	density of gas (kg/m^3)
ce	cold – hot space	ϕ	porosity in wire mesh $(-)$
ck	cold space – cooler	ω	angular speed (rad/s)
$cond$	conduction	η	efficiency $(-)$
d	displacer	ξ	coefficient of performance $(-)$
$disp$	dissipation	Δ	change in quantity
$desorb$	desorber	ε	heatexchanger effectiveness $(-)$
e	hot space	μ	dynamic viscosity (Ns/m^2)

990